Nanostructures Technology, Research and Applications

Academic and Research Staff
Prof. Karl Berggren, Dr. Rajesh Menon, Mark K. Mondol, Dr. Euclid Moon, Dr. Mark L. Schattenburg, Prof. Henry I. Smith

Visiting Scientists, Postdoctoral Associates and Research Affiliates
Prof. Maria Csete, Prof. Randy Peterson, Dr. Timothy Savas, Dr. Francesco Marsilli, Dr. Sebastian Strobel

Graduate Students
Francesco Bellei (visiting), Jae-Byum Chang, Corey Fucetola, Xiaolong Hu, Hassan Korre, Joshua Leu, Vitor Manfrinato, David Mayer, Adam McCaughan, Faraz Najafi, Sam Nicaise, Tom O'Reilly, Amil Patel, Thomas Reisinger (visiting), Jie Sun, Hsin-Yu Tsai, Lin Lee Cheong, Donald Winston.

Collaborators and NSL Users
Prof. A. Akinwande, Prof. Mark Baldo, Prof. George Barbastathis, Prof. Geoffrey Beach, Dr. Michael Bove, Prof. Ivan Celanovic, Prof. Gang Chen, Prof. Yet-Ming Chiang, Prof. Isaac Chuang, Prof. Jesus DelAlamo, Prof. Silvija Gradecak, Prof. Jarillo-Herrero, Prof. John Joannopoulos, Prof. Franz Kaertner, Prof. Leslie Kolodziejski, Prof. Jing Kong, Prof. Tomas Palacios, Prof. Rajeev Ram, Prof. Caroline Ross, Prof. Marin Soljacic, Prof. Francesco Stallacci, Prof. Edwin L. Thomas, Prof. Carl Thompson, Prof. Qiafeng Xia, Prof. Todd Hastings, Prof. Minghao Qi.

Technical and Support Staff
James Daley, Alicia Akins, Gillian Mackay-Smith

This chapter surveys the work going on in the NanoStructures Laboratory under the supervision of Profs. Henry I. Smith and Prof. Karl K. Berggren. The NanoStructures Laboratory includes the Scanning-Electron-Beam-Lithography Laboratory, which is discussed in a separate section below. The research ongoing includes work on nanofabrication and devices. The work supervised by Prof. Berggren additionally investigates the application and fabrication of devices using the foundations of quantum mechanics. We focus on: (1) superconductive devices and materials, single-photon detection and quantum computing; (2) nanofabrication methods; and (3) applications of nanofabrication to energy systems. Superconductive devices are among the most readily engineered examples of devices exhibiting quantum-mechanical effects. We therefore work with superconductive materials, including efforts in materials, processing, and analysis. Also, because quantum-mechanical effects are primarily observable at microscopic length scale, we develop and implement novel methods of nanofabrication. We take a multi-disciplinary approach to these topics, borrowing techniques from physics, electrical engineering, computer science, chemistry, and materials science. The work supervised by Prof. Smith additionally investigates micro- and nanophotonic devices, and nanoscale fabrication methods.

NanoStructures Laboratory

Sponsors:
MIT Institute Facility under RLE

Project Staff:
Mark K. Mondol, James Daley, Prof. Karl Berggren, Dr. Mark Schattenburg, Prof. Henry I. Smith

In 2006, the Nanostructures Lab converted its fabrication facility in Room 39-477 into an Institute-wide service facility under the Research Laboratory of Electronics (RLE). This facility provides

MIT and outside users with easily accessible Reactive Ion Etching (RIE), interferometric lithography, electron-beam evaporation, resist spinning, wet bench processing, scanning-electron microscopy (SEM), atomic-force microscopy (AFM) as well as a variety of associated lab tools and techniques required for nanofabrication. Access to the NSL research tools is coupled with resident expertise and advice. The facility Director is Prof. Karl Berggren. Prof. Henry I. Smith and Dr. Mark Schattenburg are Associate Directors. James Daley manages the day-to-day laboratory operations, provides training on the tools mentioned above, and student guidance on optimal nanofabrication techniques and strategies.

Projects that made use of the NSL facility during the past year included: relief templates for self assembly of block copolymers; ultra fast optical detectors; 1-D, 2-D and 3D photonic crystals; ring-resonator add/drop filters; optical-polarization splitter-rotator devices; magnetic-memory devices; quantum photodetectors; templates for nanoimprint lithography; photomasks for interferometric-spatial-phase-imaging (ISPI) alignment and gapping; 4-point contacts for measurements on nanotubes and nanowires; abosorbance modulation optical lithography and imaging; 3-D self folding structures; Si-Ge combined devices; arrays of Fresnel zone plates and thin resist exposure to investigate the ultimate limits of lithography. Use of the facility, by the MIT community encompassed: 25 Principal Investigators, 5 Departments and 4 Labs or Centers. More than 80 users were trained. In addition, two non-MIT entities utilized the lab last year.

Tools within the NSL Facility include: Zeiss 982 SEM, Novelx SEM, Digital Instruments AFM, 2 Leica optical microscopes, Plasma Therm RIE (Reactive Ion Etcher), Samco ICP RIE, optical mask aligner, UV flood exposure, Gaerntner ellipsometer, Temescal e-beam evaporator, critical point dryer, sputtering system, ion miller, rapid thermal annealer, an optical polishing tool, 3 wet benches, class 10,000 and class 100 cleanroom space, and interferometic lithography systems (Lloyd's mirror and Mach-Zehnder types, both NSL developed). There are also fume hoods, laminar flow hoods, hotplates, ovens, inspection microscopes, and a variety of hand tools and glassware required for nanofabrication. The NSL is housed in Building 39, which provides acid sinks, deionized water, dry N_2 and other building services, but has satellite laboratories with individual tools in buildings 26 and 38. The interference lithography and optical polishing are located in building 26; the scanning electron-beam lithography is located in building 38.

Scanning Electron Beam Lithography (SEBL) Laboratory

Sponsors:
MIT Institute Facility under RLE

Project Staff:
Mark K. Mondol, Prof. Henry I. Smith, Prof. Karl Berggren

SEBL Users:
Prof. Akintunde Akinwande, Prof. Dimitri Antoniadis, Prof. Raymond Ashoori, Prof. Mark Baldo, Prof. George Barbastathis, Prof. Moungi Bawendi, Prof. Geoffrey Beach, Prof. Angela Belcher, Prof. Duane Boning, Prof. Michael Bove, Prof. Vladimir Bulovic, Prof. Anantha Chandrakasan, Prof. Gang Chen, Prof. Isaac Chuang, Prof. Jesus DelAlamo, Prof. Karen Gleason, Prof. Silvija Gradecak, Prof. Paula Hammond, Prof. Pablo Jarillo-Herrero, Prof. Jongyoon Han, Prof. Judy Hoyt, Prof. Franz Kaertner, Prof. Rohit Karnik, Prof. Marc Kastner, Prof. Sang-Gook Kim, Prof. Leslie Kolodziejski, Prof. Jing Kong, Prof. Carol Livermore, Dr. Jagadeesh Moodera, Prof. Thomas Palacios, Prof. Joseph Paradiso, Prof. Rajeev Ram, Prof. Caroline Ross, Dr. Mark Schattenburg, Prof. Joel Schindall, Prof. Marin Soljacic, Prof. Francesco Stellacci, Prof. Michael Strano, Prof. Timothy Swager, Prof. Edwin L. Thomas, Prof. Harry Tuller, Prof. Fladan Vuletic, Prof. Dana Weinstein, Prof. Mehmet Yanik

In 2004, the Nanostructures Lab converted its scanning-electron-beam-lithography (SEBL) facility in Room 38-165 into an Institute-wide service facility under the Research Laboratory of

Electronics (RLE). This facility provides MIT and outside users with easily accessible e-beam lithography, coupled with resident expertise and advice. The facility is managed by Mark Mondol who provides training on the e-beam tools, direct patterning service, and advice on optimal nanofabrication techniques and strategies. The NanoStructures Laboratory (NSL) and the Microsystems Technology Laboratories (MTL) have service facilities for spin coating of resists, resist development and other forms of processing.

Projects that made use of the SEBL facility during the past year included: graphene Josephson junctions; single-photon detectors; origami 3D folding membranes; quantum dots; III-V Mosfets; patterned nanotube growth;acoustic-wave resonators; relief templates for self assembly of block copolymers; point-contact devices; 1-D, 2-D and 3D photonic crystals; ring-resonator add/drop filters; optical-polarization splitter-rotator devices; magnetic-logic devices;; templates for nanoimprint lithography; photomasks for interferometric-spatial-phase-imaging alignment and gapping; 4-point contacts for measurements on nanotubes and nanowires; III-V compound T-gate HEMTs and arrays of Fresnel zone plates. Research in lithographic processing included salty development of HSQ (Hydrogen silsesquioxane) which demonstrated improved resolution and contrast. Use of the facility, by the MIT community, was widespread, there were: 45 Principal Investigators, 7 Departments, 8 Labs or Centers, 2 non-MIT entities and 65 distinct trained users over the last year.

In previous years, two SEBL tools were available: a Raith 150 and the VS-26, which was donated in the mid 1990's by IBM. This year we were forced to decommission the VS 26 due to nonavailability of replacement parts. The laboratory is pursuing means of replacing the VS26 with a commercial system. The Raith 150 system is shown in Figure 1. Its electron-optical column is essentially identical to that of a Zeiss Gemini SEM, and provides a beam diameter as fine as 2 nm. Nested L patterns of 11 nm pitch, with linewidths ~ 5 nm have been written with the system, as illustrated in **Figure 2.** The Raith 150 includes a pattern generator and laser-interferometer-controlled stage with an integrated software package. Version 4.0 software now allows users to do automated field alignment to approximately ± 25nm. The system can operate from 1 to 30keV. Wafers up to 150 mm can be loaded into the system. Typically, users are trained for 4 to 10 hours and then allowed to operate the tool on their own. The tool is available, for most users, 24 hours a day, 7 days a week.

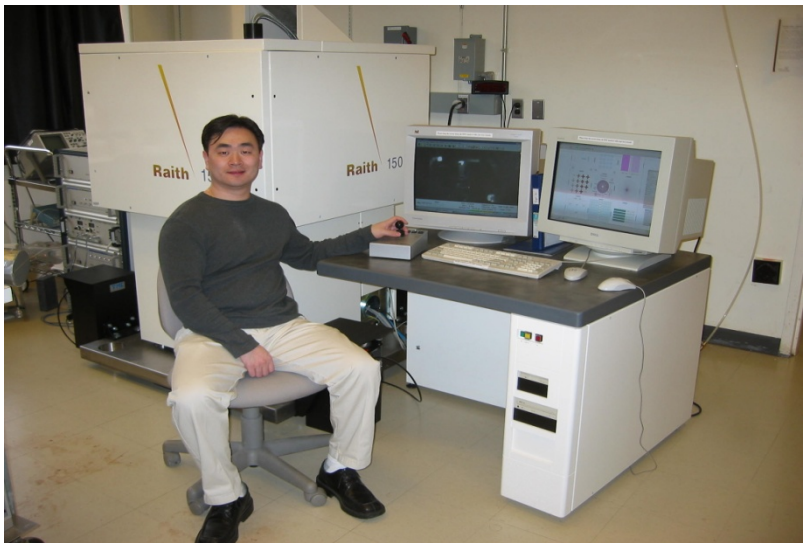

Figure 1. *The Raith-150 electron-beam lithography system. This tool provides sub-10-nm patterning resolution, and pattern-placement accuracy ~ 1nm via spatial phase locking. The operator is Dr. Feng Zhang.*

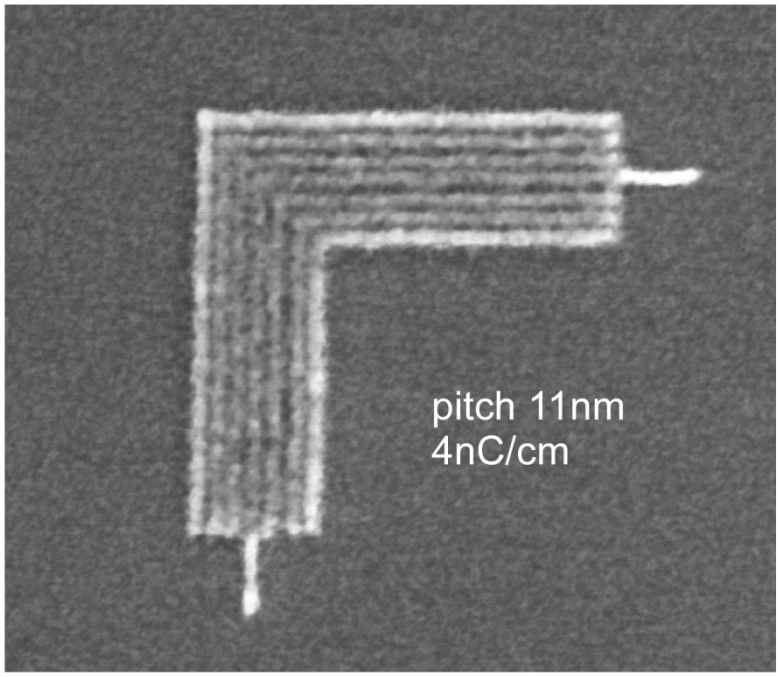

Figure 2: *Scanning-electron micrograph of exposed and developed HSQ illustrating the resolution of the Raith 150 SEBL system; 11 nm pitch, linewidth ~5nm.*

The Raith 150 is used in a program to develop spatial-phase-locked e-beam lithography, described elsewhere. The objectives of that program are to achieve sub-1 nm pattern-placement accuracy, and to reduce the cost and complexity of SEBL. In a conventional SEBL system costing several million dollars, pattern placement accuracy is typically much worse than 10 nm.
The SEBL facility encourages users with a variety of experience levels and requirements. Experienced users are able to carry out complex, multilevel aligned exposures on the Raith-150 tool. Less experienced users get hands-on instructions from facility staff, and guidance during the learning and initial fabrication stages.

Interference Lithography

Sponsors:
MIT Institute Facility under RLE

Project Staff:
Thomas B. O'Reilly, Dr. Timothy Savas and Prof. Henry I. Smith

Interference lithography (IL) is a means of rapidly creating periodic and quasi-periodic patterns that are spatially coherent over large areas. IL is a conceptually simple process, where two mutually-coherent beams of light interfere to produce a standing wave pattern that is recorded in a photosensitive material. In the most common configuration, two beams interfere forming a grating pattern, as shown in **Figure 3**. The smallest spatial-period, *P*, of a grating produced using IL is half the wavelength of the interfering light (λ), though practical issues typically require it to be slightly larger. More complex patterns, such as square or hexagonal grids, can be formed by multiple exposures or the use of more than two beams.

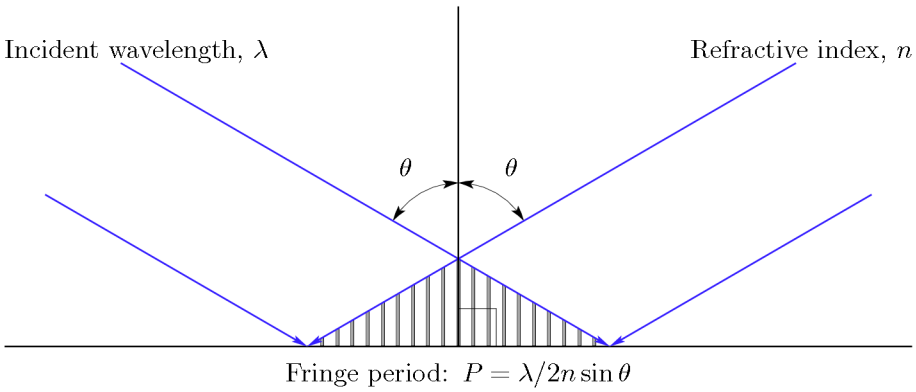

Figure 3: *Interference geometry and resulting fringe periodicity in the most common configuration, two beams incident at equal angles to the surface.*

The NanoStructures Lab has been developing IL systems and applications for over 40 years. We currently operate three different IL systems for a wide variety of applications. The IL systems have produced patterns with periods as small as 165 nm using a 325 nm Helium-Cadmium (HeCd) laser, and as small as 100 nm using a 193 nm Argon-Fluoride (ArF) laser.

One system, shown schematically in Figure 4, is configured as a Mach-Zehnder interferometer. It uses a HeCd laser with a wavelength of 325 nm. In this system, the beams are spatially filtered to ensure good spatial coherence. The absence of optical elements after the spatial filters eliminates distortion and coherent noise that might result from the use of collimating lenses, resulting in high quality fringe patterns. The use of spherical waves to form the interference pattern produces gratings whose lines follow hyperbolas, rather than straight lines, though the deviation is small, with the period varying from what would be produced by planes waves by only a few tenths of a percent over typical exposure areas. Although small, distortions of this scale can be significant, especially in metrological applications such as the fiducial grids for spatial-phase-locked electron-beam lithography. In addition to writing grids and gratings, this system has been used to measure grating distortion using a technique known as holographic phase-shifting interferometry (HPSI). With this technique, in-plane distortion of gratings and grids can be measured with a resolution of a few nanometers.

The Lloyd's mirror interferometer, shown schematically in Figure 5, also uses a 325 nm HeCd laser. A single spatial filter is located 2 meters from the substrate. The substrate and a mirror perpendicular to it are illuminated such that part of the incoming light is reflected back to the substrate. Optically, the Lloyd's mirror system is similar to the Mach-Zehnder system, except that instead of light reaching the substrate from two separate spatial filters, it comes from one spatial filter and its mirror image. In addition to reducing the complexity of the optics, the fringes formed by the Lloyd's-mirror system are stable enough that no fringe-locking is required, making the system both simpler to operate and more robust. A major advantage of the Lloyd's mirror over a Mach-Zehnder style IL system is the ease with which the spatial period of the patterns produced can be changed. The substrate holder and mirror are mounted on a rotation stage. By rotating this stage, the interference angle can be quickly changed to write patterns with periods ranging from many microns down to about 165 nm. In comparison, changing the period of a Mach-Zehnder system requires considerable effort and skill to realign numerous optical elements.

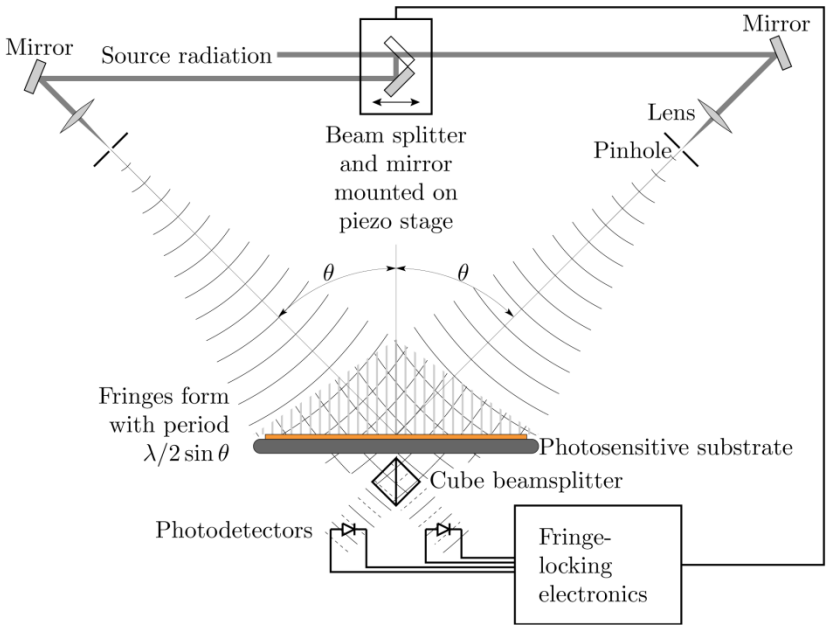

Figure 4: *Schematic of the Mach-Zehnder interference-lithography system. This setup can be used as an interference lithography system to write reference grids, as well as a holographic-phase-shifting interferometer to measure grid distortion.*

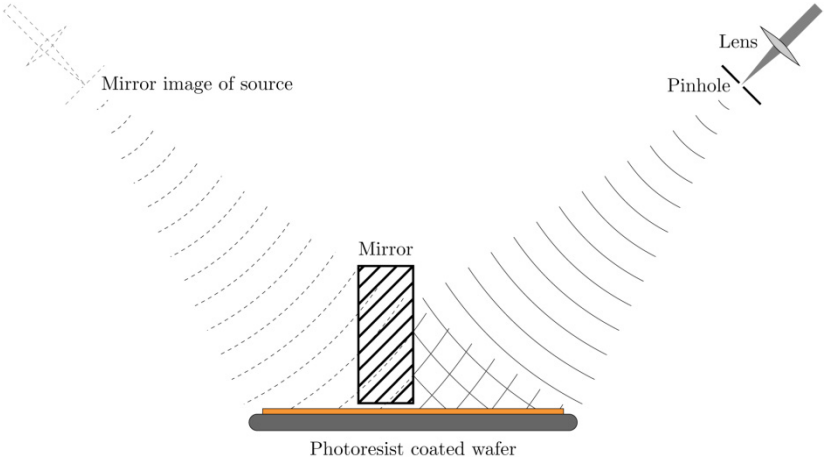

Figure 5: *Schematic of a Lloyd's mirror interferometer. The substrate and mirror are fixed at a 90˚ angle to one another, and centered in a single incident beam. Rotating the substrate/mirror assembly varies the spatial-period of the exposed grating.*

The ease-of-use and flexibility of the Lloyd's-mirror system make it possible for a large number of researchers to use the system for their own research. The Lloyd's mirror has been used for such diverse research projects as patterned magnetic media and MRAM (magnetic random access memory) devices, semiconductor quantum dots, and patterning for studies of templated self assembly of block copolymers, metal particles and nanowires. Distributed feedback (DFB) structures for quantum dot lasers and photonic bandgap devices have also been made using the system. In addition, the system has been used to develop new methods of characterizing photoresist performance.

We also operate an achromatic-interference-lithography system (AIL), to write patterns with spatial periods of 100 nm using light from a 193 nm ArF excimer laser. The AIL, shown schematically in Figure 6, is configured in such a way that the contrast of the grating image formed is largely independent of the spatial and temporal coherence of the source, allowing large-area gratings to be written with a source that has limited temporal and spatial coherence. In this configuration, the spatial period of the exposed grating is dependent only on the period of the parent gratings. Thus, gratings and grids produced with this tool are extremely repeatable. Figure 6 also shows a 100 nm-period grid of 13 nm-diameter posts etched into silicon, produced with achromatic interferometric lithography (AIL) and a sequence of etching steps. Applications of AIL have included patterned magnetic media, free-standing gratings for atom-beam interferometry, and patterns for templated self-assembly.

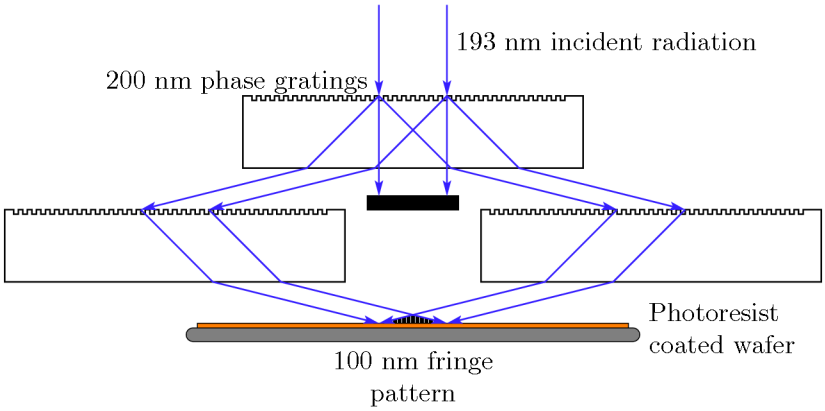

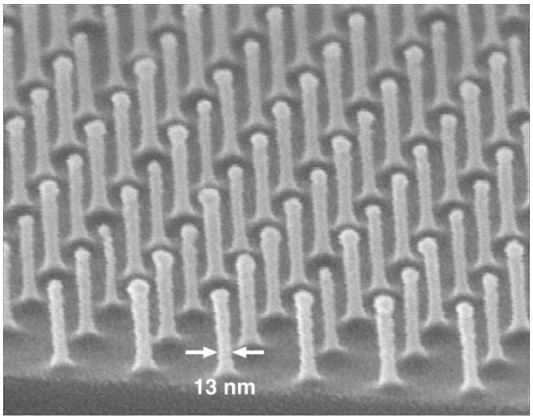

100nm-period posts in Si

Figure 6: *(Top) Achromatic interferometric lithography (AIL) configuration used to produce 100 nm-period gratings and grids. (Bottom) Scanning electron micrograph of a 100 nm-period grid, exposed in PMMA on top of an antireflection coating, and transferred into silicon by reactive ion etching and $Si0_2$ etching.*

The NSL is closely associated with the Space Nanotechnology Lab (SNL), which operates two interference-lithography systems. One is a Mach-Zehnder-type interferometer that is configured to allow very consistent and repeatable result; this system is capable of producing metrological-quality gratings and grids up to 100 mm in diameter at spatial periods down to 200 nm. The most notable applications for gratings produced with this system is the Chandra x-ray astronomy satellite launched in August of 1999 which included hundreds of matched, high-precision gratings in thick gold for high contrast at x-ray wavelengths. SNL also operates a more advanced system, called the NanoRuler, based on scanning-beam interference lithography. This system produces gratings over substrates up to 300 mm diameter with nanometer-level precision.

References:
Thomas B. O'Reilly and Henry I. Smith, "Photoresist characterization using double exposures with interference lithography," J. Vac. Sci. Technol. B, 26, 128 (2008).

Thomas B. O'Reilly and Henry I. Smith, "Linewidth uniformity in Lloyd's mirror interference lithography systems," J. Vac. Sci. Technol. B, 26, 2131 (2008).

Interference lithography with absorbance modulation

Sponsors:
Lincoln Lab Integrated Photonics Initiative

Project Staff:
Thomas B. O'Reilly, Dr. Rajesh Menon, and Prof. Henry I. Smith

In the simplest type of interference lithography (IL) system, two mutually coherent beams of light interfere to form a periodic standing wave pattern that can be recorded on a photosensitive substrate. The minimum period of the pattern that can be produced is restricted to half the wavelength of the light used. While shorter wavelength sources are available, the properties of short wavelength lasers are not always suitable for use in interference lithography. As a result, there is great interest in finding ways to write patterns with periods below the diffraction limit, so that fine-pitch patterns can be written over large areas with sources that are easy to work with. We are pursuing an approach to patterning below the diffraction limit by combining a dual-wavelength IL (DWIL) system and absorbance-modulation technology [1].

The key difference between conventional lithography and lithography using absorbance-modulation is that a polymer film containing photochromic molecules is applied on top of the photoresist. The photochromic molecules in this absorbance modulation layer (AML) can be switched between two isomeric states by exposure to two different wavelengths of light. An example of such a material is bis(bithienylethene) (BTE) which has two forms, as shown in Fig. 7.

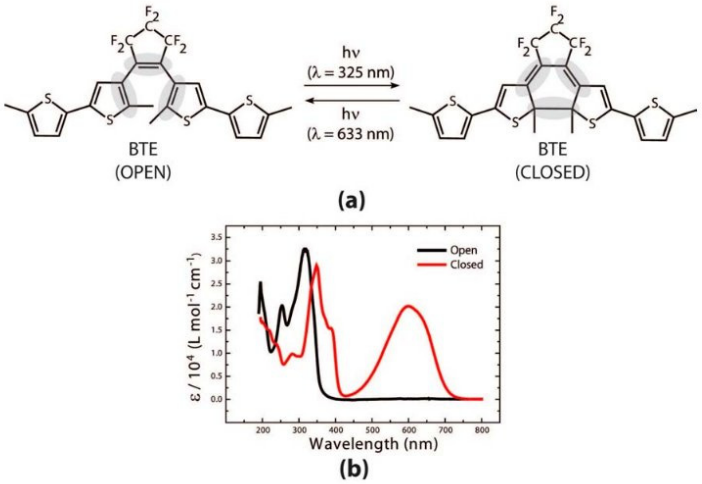

Figure 7: *Molecular structure of the open and closed states of BTE. Exposure to UV wavelengths causes BTE to switch to the closed state, while exposure to longer wavelengths, (red light for example) causes BTE to switch to the open state.*

As shown in the absorbance spectra for BTE in Fig. 7, exposure to UV light around 300-350 nm switches BTE to the closed form, which makes it more transparent to UV. In contrast, exposure

to red wavelengths switches BTE to the open form, making it less transparent to UV light. If an AML containing BTE is simultaneously exposed to standing waves in both UV and red wavelengths, as depicted in Fig. 8, it is possible to set up dynamic competition between the open and closed states, forming regions in the AML, with widths much smaller than the one-forth the wavelength, that are transparent to UV light. These regions effectively serve as subwavelength apertures in the AML through which the photoresist can be exposed by the UV wavelength.

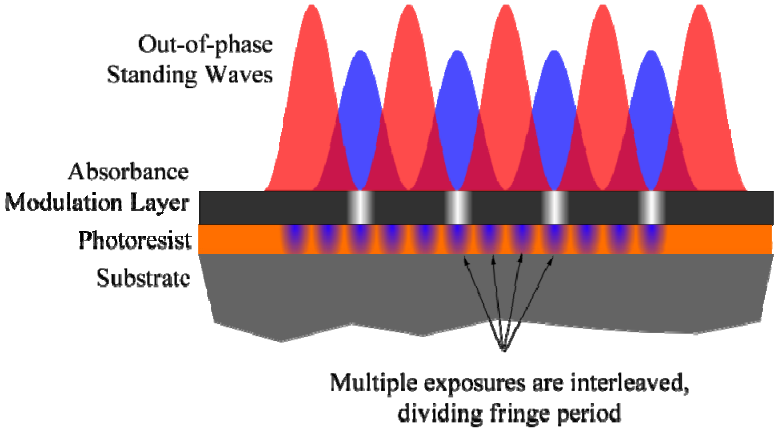

***Figure 8**: Schematic of overlaping red and UV (shown in blue) wavelengths on an absorbance modulation layer. Out-of-phase standing waves formed by the two wavelengths result in the formation of narrow regions at the null of the red standing wave that are transparent to the UV light which serves to expose the photoresist. The AML narrows the width of the exposed regions compared to what would be possible with conventional IL exposures.*

The AML alters the distribution of the exposure dose reaching the photoresist layer, narrowing the exposed regions. Since the states of the molecules in the AML are reversible, it is possible to shift the sets of fringes on the substrate, forming a new set of subwavelength apertures, and exposing a new set of lines in the resist. Because the width of the exposed resist region is reduced by the AML, it is possible resolve multiple, interleaved exposures in the resist; this is not possible in conventional IL. For example, if the initial spatial period were 400 nm, four exposures could be performed, shifting the fringes by 90 degrees after each exposure, to reduce the final period of the pattern to 100 nm. Ultimately, the extent to which the period can be divided will be limited by the performance of both the absorbance modulation layer and the photoresist.

To provide a thorough understanding of the interaction of the materials used with the exposure parameters, and their effect on the exposure results, a rigorous computer model of the DWIL exposure process has been developed. An obvious use of this model is to determine, for an existing AML material, the exposure parameters (including exposure time and intensity ratio) that will give the optimal exposure results. In addition, the simulation can be used to study how exposure results change with the optical properties of the AML. This can be used to determine what optical properties will be needed to achieve deep, sub-wavelength resolutions. This information can be used to guide the development of new materials for use with absorbance modulation. Based on rigorous-coupled wave analysis, this simulation models the interaction of two different wavelengths of light with the AML, the photoresist and the substrate.

The model discretizes the AML, and then calculates the electric-field throughout the resist-AML stack, which is used to calculate how the state of the AML changes in response to the exposure. An iterative process is used to model how the field changes with time, which can be used to calculate the exposure received by the resist. The exposure process can be simulated either for a specific exposure time, or until steady state conditions are reached. Combined with a

photoresist exposure model, the simulation can be used to predict the results of multiple exposures to determine the final spatial resolution that can be achieved.

We have developed a concept for a DWIL system to be used both to test materials and to provide sub-100 nm periods using relatively long wavelength laser sources. This system, shown schematically in Fig. 9, will form two standing waves, one using 325 nm light from a helium-cadmium laser and a second from a longer wavelength, red laser. In essence, the system consists of two independent Mach-Zehnder style IL systems, simultaneously illuminating the same substrate.

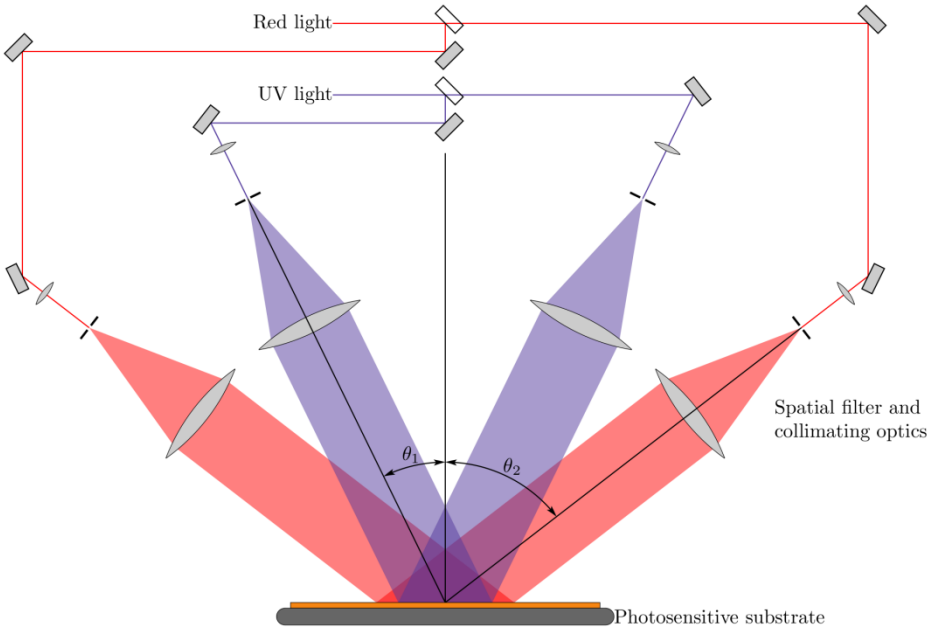

Figure 9: *Schematic of a dual-wavelength IL (DWIL) system. Beams of two different wavelengths are split, expanded and collimated to simultaneously form standing waves of the same period but shifted in spatial phase.*

A challenge in the implementation of a DWIL system is to match the period of the two standing waves and control their relative phase. This will be accomplished through the use of a reference grating placed next to the exposure area, with a period twice the period of the fringes being formed by the DWIL system. When the incident UV and red beams are properly aligned, light from each of the four incident beams is diffracted in a direction normal to the surface of the reference grating, as shown in Fig. 10. Interference between the two normally diffracted orders of each wavelength forms a pattern that can be used both to ensure that the periods of the two fringe patterns match and to control the phase of the standing wave pattern relative to the phase of the reference grating.

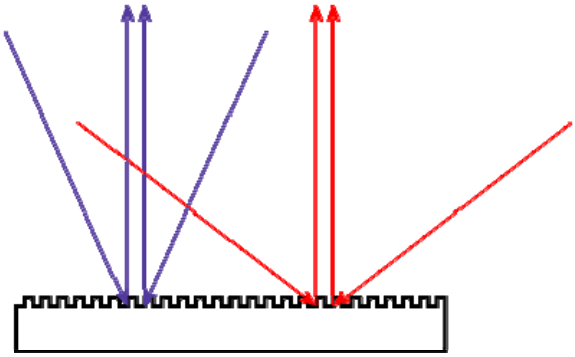

***Figure 10**: Schematic of the reference grating, which is mounted next to the exposure area. The period of the reference grating is twice the period of the fringes being written. When the incident beams are properly aligned, light from each of the wavelengths diffracts in a direction normal to the surface of the reference grating.*

References

[1] Rajesh Menon and Henry I. Smith, "Absorbance-modulation optical lithography," J. Opt. Soc. Am. A **23**, 2290-2294 (2006).

Microscopy Beyond the Diffraction Limit Using Absorbance Modulation

Sponsors

MIT Deshpande Center

Project Staff

Dr. Rajesh Menon, Hsin-Yu Tsai, Prof. Henry I. Smith

Absorbance-Modulation Imaging (AMI) is an approach to overcoming the optical diffraction limit in the far–field, to achieve macro-molecular resolution with visible-light photons. AMI relies on an absorbance-modulation layer (AML), composed of photochromic molecules, in contact with the object under study. Illumination at one wavelength, λ_2, renders the AML opaque, while illumination at a shorter wavelength, λ_1, renders it transparent. When illuminated with a ring-shaped spot at λ_2 co-incident with a focused spot at λ_1, the dynamic competition results in a nanoscale aperture, through which λ_1 can penetrate to the substrate beneath, as illustrated in Figure 11. The size of the aperture is limited only by the photo-kinetic parameters of the AML and the intensity ratio of the two illuminating wavelengths, not their absolute intensities [1]. By scanning this dynamic nanoscale aperture over the sample, resolution beyond the far-field diffraction limit is achieved. A related technique, called stimulated-emission-depletion (STED) fluorescence microscopy was demonstrated by S. Hell et al. [2]. However, while STED requires high power pulsed illumination and fluorescent markers, AMI can operate at low illumination intensity and does not require fluorescent markers. A schematic of an AMI microscope is shown in Figure 12, in which collimated beams at λ_1 and λ_2 illuminate an array of microlenses which consists of a binary phase element that creates a doughnut-shaped spot at λ_2 and a round spot at λ_1[3,4].

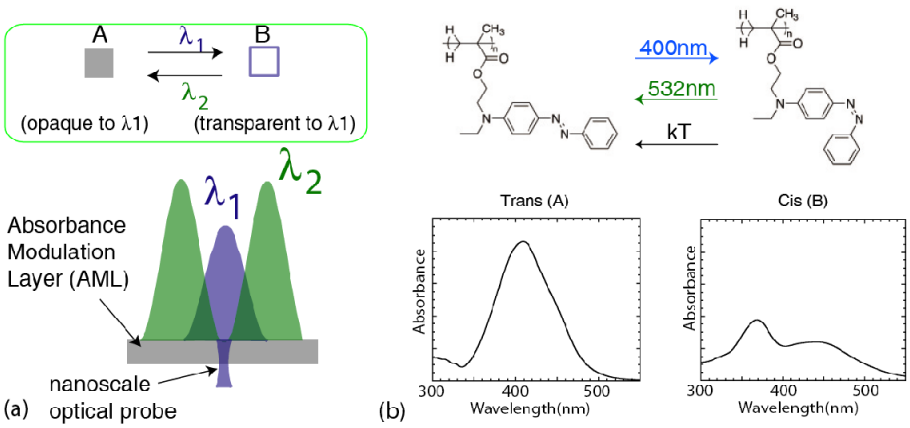

Figure 11: *(a) Concept and illumination configuration for absorbance modulation. Through dynamic competition of the reversible transitions in the AML, the ring illumination at λ_2 creates a sub-wavelength aperture for λ_1. (b) An example of an AML composed of a polymer containing the photochromic azobenzene side chain is shown at the top. Upon exposure to 400 nm light, the trans isomer undergoes a photoisomerization reaction forming the cis isomer. The reverse reaction is favored upon exposure to 532 nm light or thermal excitation. The absorbance of the two isomers at λ_1=400 nm are markedly different.*

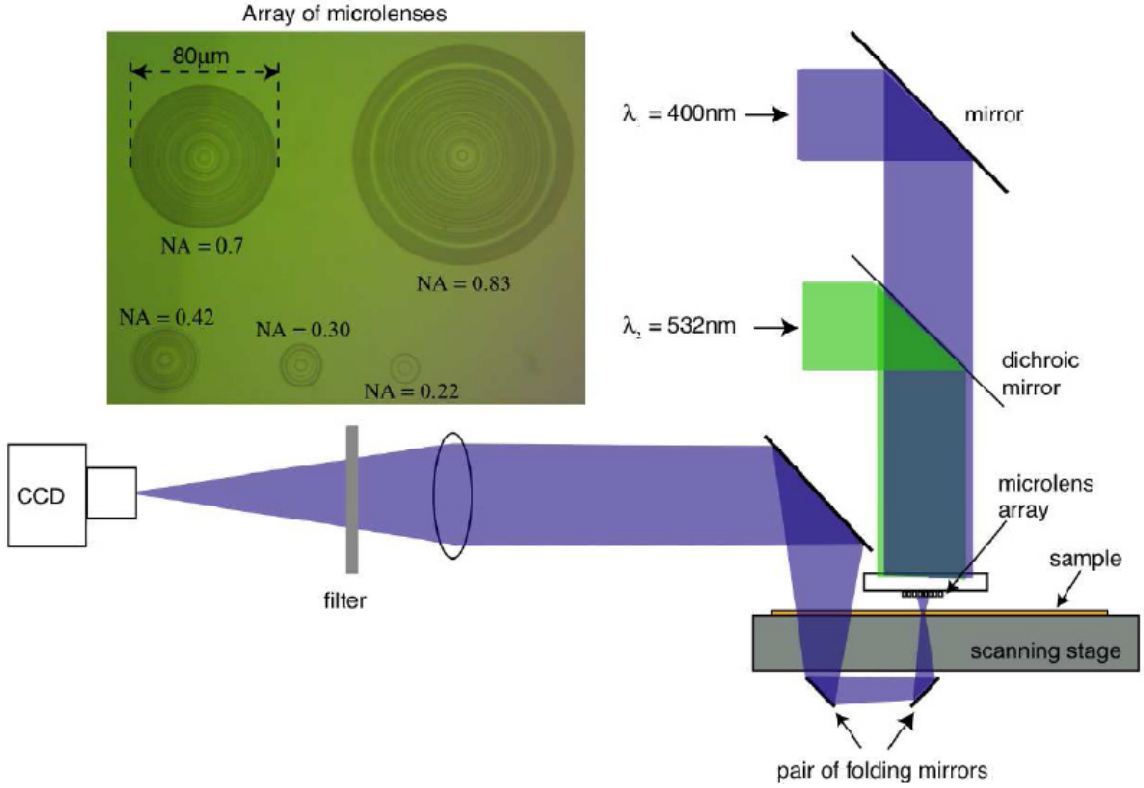

Figure 12: *Schematic of the absorbance-modulation imaging (AMI) system. The inset on the left shows an optical image of the microlenses of various numerical apertures (NAs). The microlenses are binary diffractive-optical elements that focus λ_1 = 405nm illuminations into round-shaped spots and λ_2 = 532nm illuminations into doughnut-shaped spots at a focal plane 40um below the plane of the microlens array. In combination of an overlayer of 220nm azobenzene polymer coated on the sample, nanoscale optical probes are produced at the top surface of the sample. The scanning stage has a clear aperture to allow collection of transmitted light. The microlenses are spaced such that the signals are read out in parallel. The λ_2 beam is not shown past the sample for clarity.*

Imaging results of two types of samples are shown below: dense line/space patterns of metal on glass and nanoparticles with a known mean size (both overcoated with 220nm of the azobenzene polymer, i.e. the AML.)

Figure 13(A) shows transmission images of a 500nm-period grating pattern obtained using a microlens of numerical aperture (NA) = 0.83. On the top and bottom are images taken with only λ_1 (λ_1 = 405nm) illumination and with both λ_1 and λ_2 (λ_2= 532nm) illumination. Figure 13(B) shows the averaged linescan of the images in Fig. 13(A). Even at relatively low peak intensities at λ_2 (0.4W/m^2), it is clear that absorbance modulation increases the image contrast. The contrast is defined as the difference between the maximum and minimum signal values over the average signal value.

Figure 14 shows images of nanoparticles on glass when the intensity ratio of λ_2 to that at λ_1 is large enough to achieve highly compressed optical probes. Figure 14(A) is a schematic of the sample being imaged. The sample consisted of 100nm gold nanoparticles. The images were taken with a microlens of NA = 0.7 with only λ_1 (B), and with both λ_1 and λ_2 (C). Gaps between the nanoparticle clusters as small as 78nm are resolved when both wavelengths are used. Figures 14(D)–4(F) show images of the same region on a glass slide with dispersed 10nm gold nanoparticles, taken at different ratios of the peak focal intensity at λ_2 to that at λ_1 (I_{2peak}/I_{1peak}). As the I_{2peak}/I_{1peak} ratio increases, the size of the probe decreases and finer structural details are revealed.

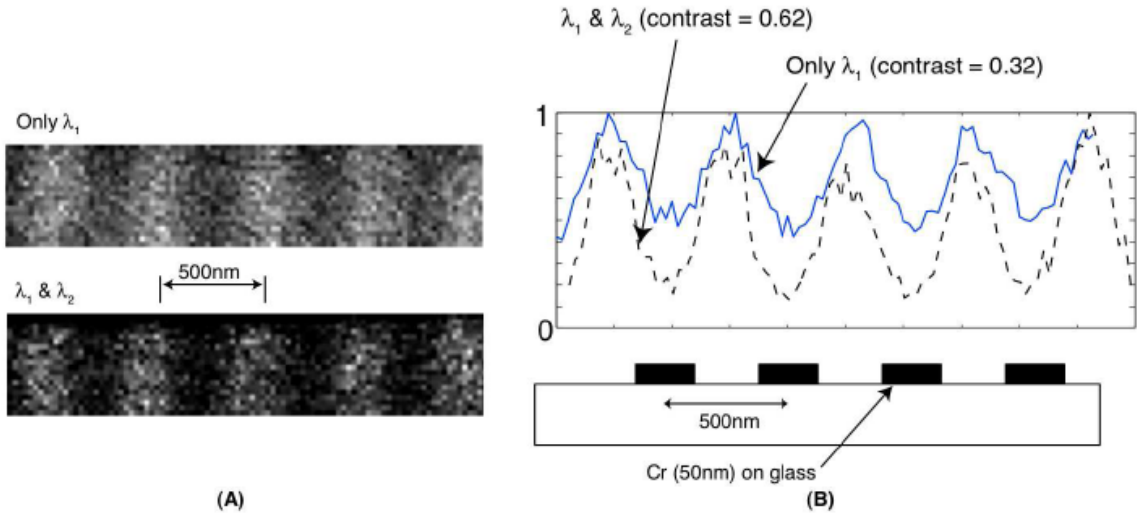

Figure 13: *Absorbance-modulation imaging of a 500nm-period metal grating. (A) Transmission images taken with only λ_1 = 405nm (top) and with both λ_1 = 405nm and λ_2 = 532nm (bottom). (B) Average linescans through the images in (A). The solid line shows the scan with only λ_1 illumination, whereas the dashed line depicts the scan with simultaneous illumination of both λ_1 and λ_2 beams. The image contrast is increased by a factor of ~2 because of absorbance modulation. The sample consisted of 50nm-thick layer of chromium on glass and was overcoated with 220nm of the azobenzene polymer. The numerical aperture (NA) of the microlens was 0.83.*

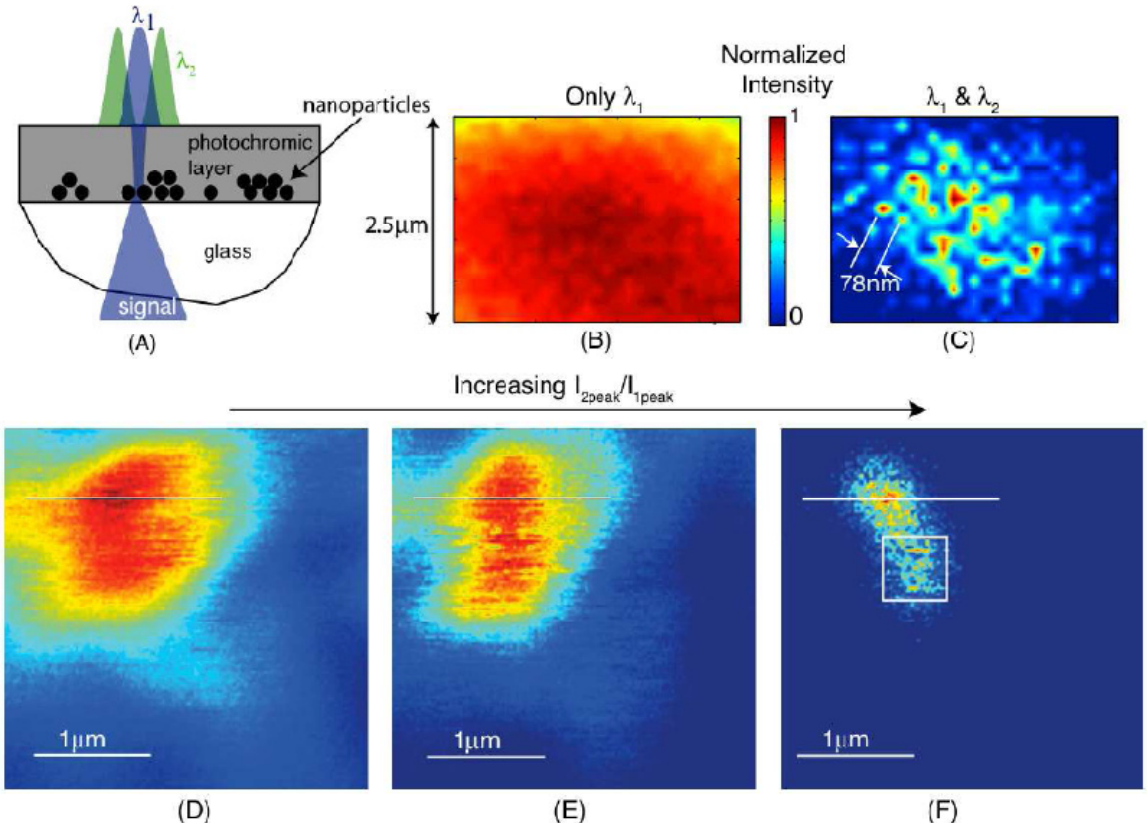

Figure 14: *(A) Schematic of sample, a glass slide with gold nanoparticles randomly dispersed on the surface. The slide was coated with 220nm of the azobenzene polymer. (B)-(C) Transmission images of 100nm gold nanoparticles taken by a microlens of NA = 0.7 with only λ_1 = 405nm (B) and with both λ_1 = 405nm and λ_2 = 532nm (C). (D)-(F) Transmission images of 10nm gold nanoparticles dispersed on a glass slide taken with a microlens of NA = 0.55. As the ratio of the intensity at λ_2 to that at λ_1 increases (from (D) to (F)), nanoscale structural details are revealed.*

References

R. Menon and H. I. Smith, "Absorbance modulation optical lithography," *J. Opt. Soc. Am. A* 23(9): 2290-2294 (2006).

S.W. Hell and J. Wichmann, "Breaking the diffraction resolution limit by stimulated emission: stimulated-emission-depletion fluorescence microscopy," *Optics Lett.* 19(11): 780-782 (1994).

R. Menon, P. Rogge, and H.-Y. Tsai, "Design of diffractive lenses that generate optical nulls without phase singularities," *J. Opt. Soc. Am. A*, 26(2): 297-304 (2009).

Hsin-Yu Tsai, Henry I. Smith, and Rajesh Menon, "Reduction of focal-spot size using dichromats in absorbance modulation," *Optics Letters*, 33(24), 2916 (2008).

Hsin-Yu Tsai, Samuel W. Thomas, and Rajesh Menon, "Parallel scanning-optical nanoscopy with optically confined probes," Optics Express, 18(15), 16014 (2010).

Spatial-Phase-Locked Electron-Beam Lithography at Low Beam Energies

Sponsors
National Science Foundation

Project Staff
Dr. Euclid E. Moon, Lin Lee Cheong, Prof. Henry I. Smith, Prof. J. Todd Hastings (U. Kentucky)

Our research in spatial-phase-locked electron-beam lithography (SPLEBL) is conducted in collaboration with the University of Kentucky. It is aimed at reducing pattern-placement errors in scanning electron-beam-lithography systems to the sub-1 nm level. Such high precision is essential for certain applications in photonics and nanoscale science and engineering. SPLEBL is currently the only approach capable of achieving such pattern-placement accuracy. As shown in Fig. 15, SPLEBL uses a periodic signal, derived from the interaction of the scanning e-beam with a fiducial grid placed directly on the substrate, to continuously track the position of the beam while patterns are being written. Any deviation of the beam from its intended location on the substrate is sensed, and corrections are fed back to the beam-control electronics to cancel beam-position errors. In this manner, the locations of patterns are directly registered to the fiducial grid on the substrate.

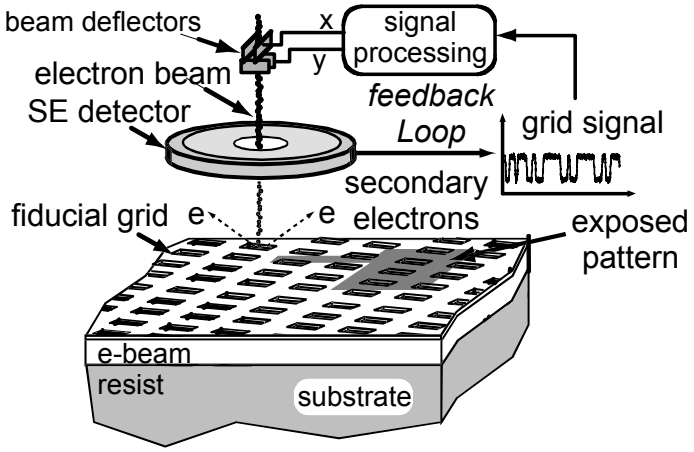

Figure 15: Schematic of the global-fiducial-grid mode of spatial-phase-locked electron-beam lithography. The periodic signal detected from the fiducial grid, which includes both X and Y components, is used to measure placement error, and a correction signal is fed back to the beam-deflection system.

The research effort at MIT is now focused on developing the materials and processes for producing the fiducial grid, with the objectives of: maximizing the area and absolute accuracy of the grid; minimizing electron scattering from the grid, which would be deleterious to precision lithography; modulating the secondary-electron signal with the thinnest possible grid material; and minimizing the cost and inconvenience of producing the grid on substrates of interest. To produce grids over large areas with high accuracy we employ various forms of interference lithography, including Mach-Zender, and Scanning-Beam Interference Lithography (SBIL).

In order to implement SPLEBL at beam energies in the 1 to 2 keV range, it is important to minimize electron scattering. The current approach to grid fabrication addresses this issue through modulation of the secondary-electron signal by very thin layers of material, including single-molecule layers. Previoius research has shown the potential of self-assembled molecular layers of 1-octadecanethiol (ODT) or 3-amino-propyl-triethoxy-silane (APTES) as the grid material. However, formation of an ODT monolayer depends upon attachment of a sulphur end-chain to a gold layer on top of the e-beam resist. Gold, even in a nanometer-thick layer, is

undesirable because of its high electron-scattering cross-section. APTES attaches well to metals such as aluminum (Z=13), which reduces, but does not eliminate, the problem of scattering. Here we investigate an alternative method to modulate secondary-electron signals via a grid composed of low-atomic-number (average Z<4) polymers in an extremely thin layer.

As shown in Fig.16, PFI-88 resist can be thinned with heptanone to 11 nm (1:10 PFI-88:heptanone) at 3k RPM spin speed. Figure 17 is a plot of the secondary-electron (SE) signal level for several resist thicknesses, and a comparison with a single self-assembled molecular layer of APTES. Although the SE level is relatively high in this particular sample, APTES is subject to variable and uncontrollable SE yield associated with aluminum oxide growth. Resist spinning is intrinsically advantageous since it allows controlled, repeatable thicknesses. As indicated in Fig. 17, SE levels from PFI-88 are directly related to thickness, providing a new level of control over the contrast between the grid and an underlying material.

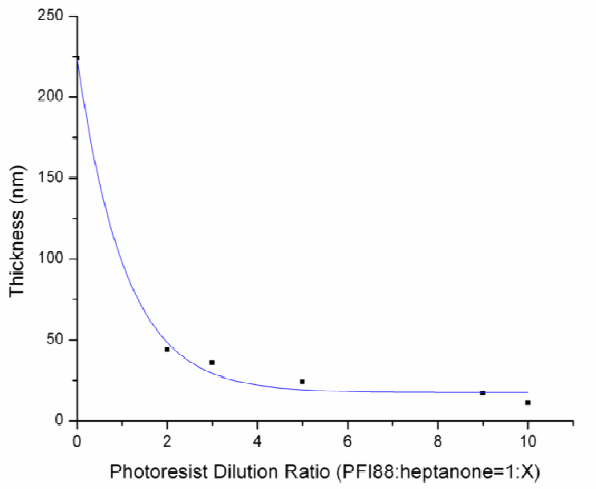

Figure 16: Plot of the thickness of PFI-88 as a function of dilution ratio in heptanone.

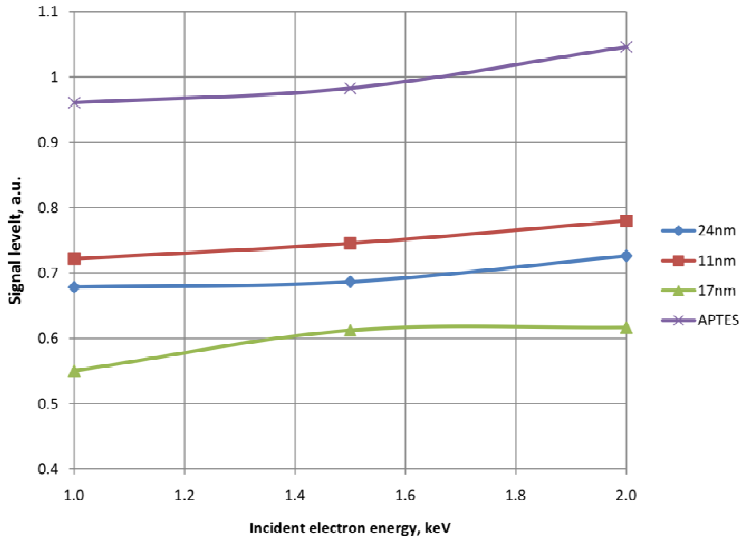

Figure 17: Plot of the secondary-electron return from PFI-88 resist, for several layer thickness, as a function of incident electron beam energy. PFI-88 resist layers and APTES monolayers are on silicon substrates. The reference level of 1 is set to a clean, bare Si surface included in the same scan line as the PFI-88. A Faraday cup, also in the same scan line, is used to set the zero level. Secondary-electron signal levels are dependent on the resist thickness, indicating the ability to use the resist thickness to control SE contrast.

Figure 18 shows a secondary electron image of a fiducial grid made with a thinned PFI-88 resist, patterned over a large area using interference lithography.

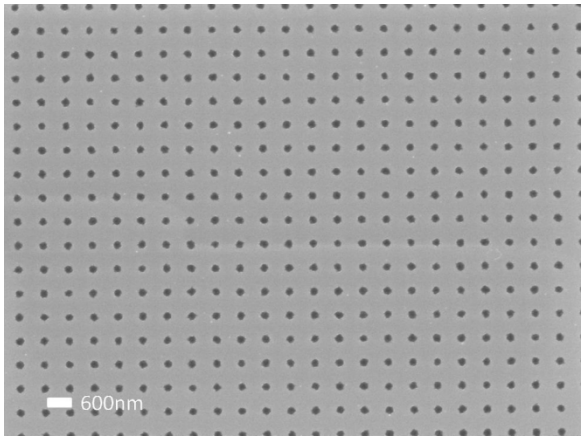

Figure 18: SEM micrograph of a fiducial grid exposed in thinned PFI-88 photoresist. The dark regions correspond to the resist; the light regions are silicon.

References

J.T. Hastings, F. Zhang, and H.I. Smith, "Nanometer-level stitching in raster-scanning e-beam lithography using spatial-phase locking," *J. Vac. Sci. Technol.* B, **21**, 2650 (2003).

F. Zhang, H.I. Smith and J.F. Dai, "Fabrication of high-secondary-electron-yield grids for spatial phase-locked electron-beam lithography," *J. Vac. Sci. Technol.* B, **23**, 3061 (2005).

A.V. Krishnamurthy, R.V. Namepalli, and J.T. Hastings, "Subpixel alignment for scanning-beam lithography using one-dimensional, phase-based mark detection," *J. Vac. Sci. Technol.* B, **23**, 3037 (2005).

J.T. Hastings, "Real-time determination of electron-beam probe shape using an *in situ* fiducial grid," *J. Vac. Sci. Technol.* B, **24**, 2875 (2006).

Y. Yang and J.T. Hastings, "Real-time spatial-phase locking for vector-scan electron beam lithography," *J. Vac. Sci. Technol.* B, **25**, 2072 (2007).

C.B. Samantaray and J.T. Hastings, "Self-assembled monolayer fiducial grids for spatial-phase-locked electron-beam lithography," *J. Vac. Sci. Technol.* B, **26**, 2351 (2008).

Y. Yang and J.T. Hastings, "Field-programmable gate array implementation of real-time spatial-phase locking for electron-beam lithography," *J. Vac. Sci. Technol.* B, **26**, 2316 (2008).

C.B. Samantaray and J.T. Hastings, "The effect of thin metal overlayers on the electron beam exposure of polymethyl methacrylate," *J. Vac. Sci. Technol.* B, **26**, 2300 (2008).

C.B. Samantaray and J.T. Hastings, "Amino-propyl-triethoxy-silane on aluminum fiducial grids for spatial-phase-locked electron-beam lithography," *J. Vac. Sci. Technol.* B, **27**, 2558 (2009).

Design and Fabrication of Sampled Bragg Gratings in SOI

Sponsors:
DARPA

Project Staff:
Jie Sun, Charles W. Holzwarth, Prof. Henry I. Smith

Bragg gratings are widely used in optical communication systems. In order to introduce a phase shift or a chirp, Scanning-Electron-Beam-Lithography (SEBL) is used. It is often difficult to achieve the required precision in such writing. For this reason, we developed a novel sampled-Bragg grating (SBG) structure to realize various grating responses using low cost optical lithography. Interference lithography is used to fabricate a uniform base grating with excellent spatial phase coherence. This grating is then iamplitude modulated to achieve various grating responses, such as an equivalent of a quarter-wave phase-shift.

A schematic diagram of the SBG is shown in Fig. 19. Various grating responses can be realized by allocating the sampling positions and by varying the duty cycle of each sampling. For example, the phase shift grating is achieved by phase shifting the sampling instead of the grating itself. Figure 20(a) shows the simulated transmission spectrum of a phase shift grating using SBG, where the desired filter response appears in the -1st channel.

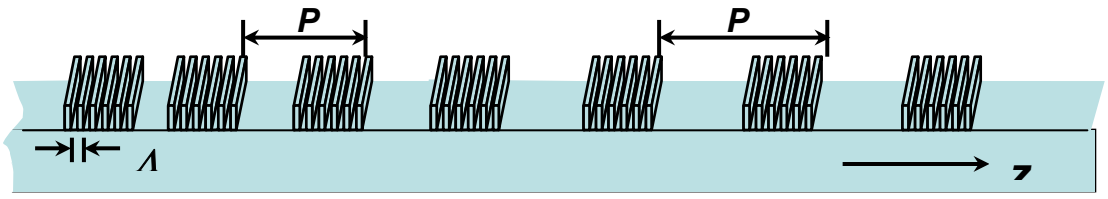

Figure 19: Schematic of the Sampled Bragg grating (SBG)

The sampling period is usually much larger than the grating period, enabling use of optical-contact lithography to fabricate the sampling. To demonatrate the SBG experimentally, we first deposit a thin layer of SiO_2 on top of an SOI wafer. The base grating was formed on this layer with interference lithography and reactive ion etching. This SiO_2 grating will serve as a hard mask to etch the grating into silicon. The sampling pattern was transferred onto the grating layer by optical-contact lithography and the excess background grating eched away. A second contact lithography and HBr etching patterned the ridge waveguide. Finally, the grating pattern was etched into the top of the silicon ridge waveguide. Figure 21 shows micrographs of a fabricated SBG. Figure 20(b) shows the measured transmission spectrum. Results are similar to the simulation in Fig. 20(a).

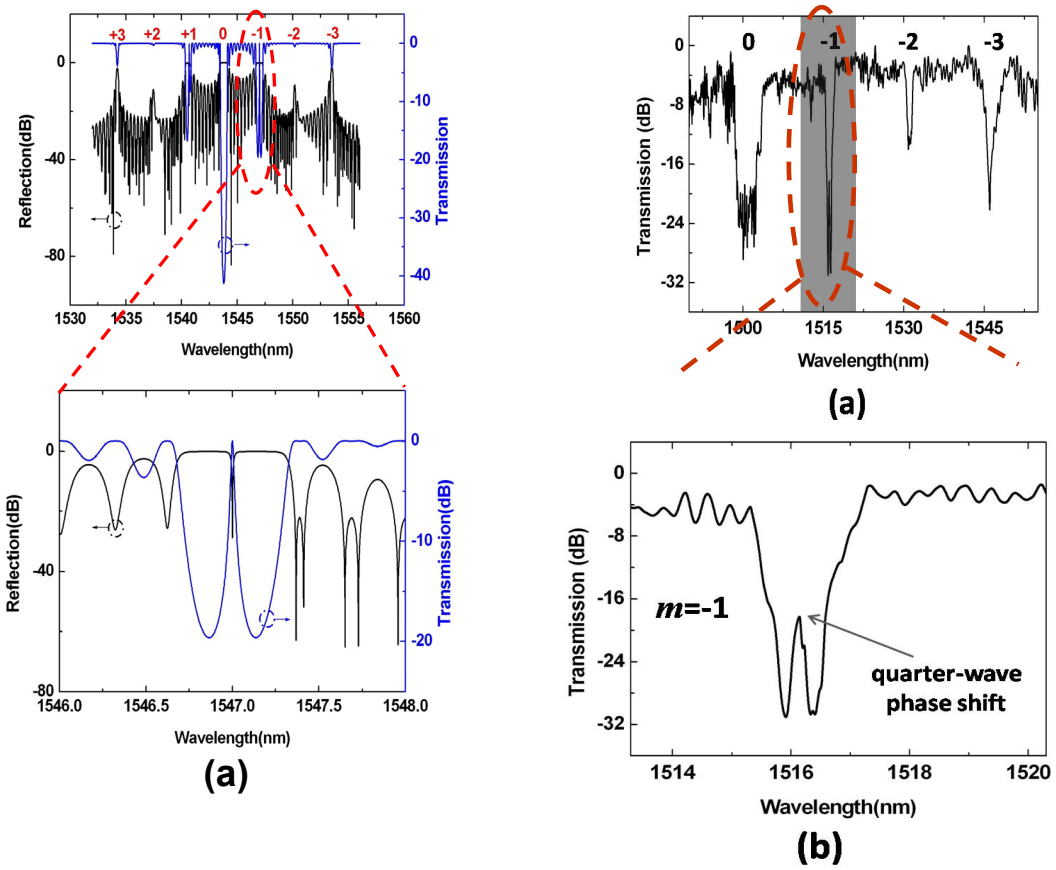

Figure 20: Filter responses of a π-phase shift grating using SBG technique (a) simulated; (b) measured

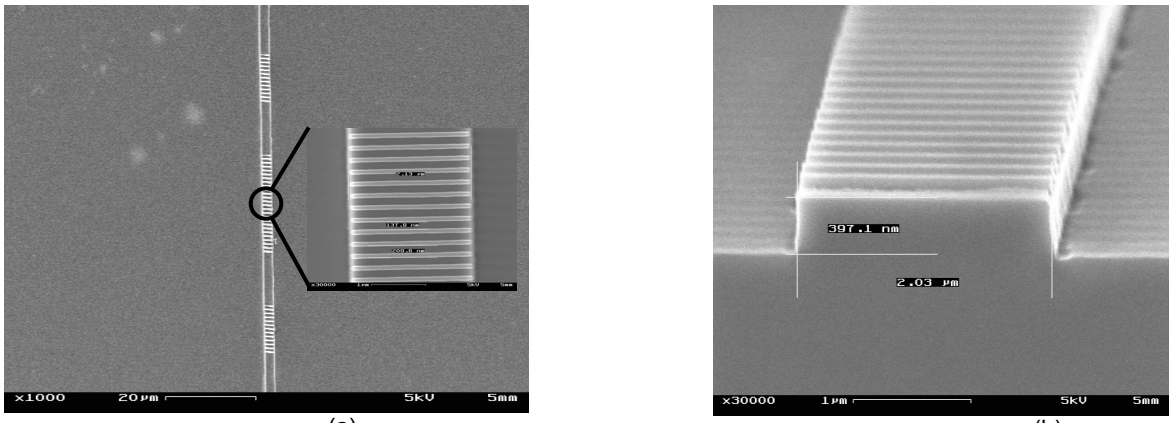

(a) (b)

Figure 21: (a) SEM images of a fabricated SBG, (b) cross-sectional view of the SBG

Fabrication of 3-Dimensional Nanostructures by Stacking Pre-patterned membranes

Sponsors:
AFOSR via MURI; in collaboration with Purdue University

Project Staff:
Corey Fucetola, Lin Lee Cheong, Shabnam Ghadar ghadr, Dr. Euclid Moon, Professor Henry I. Smith

The planar fabrication process, i.e., lithography followed by pattern transfer, which has enabled integrated electronics and photonics, is fundamentally 2-dimensional. That is, patterns are formed only in the focal plane of a lithographic system. Complex three-dimensionally-patterned structures can be achieved through layer-by-layer buildup, but such processes tend to be tedious and low yield. In this project we aim to develop an entirely new approach to building three-dimensional structures, based on patterning thin membranes and then stacking them in multiple layers bonded together. In this way, patterned membranes can be inspected, and defective ones discarded, before stacking them into 3D structures. Our initial objective is to fabricate large 3D photonic-crystals with internal devices such as slow-light structures and, at a later stage, lasers.
Photonic crystals are periodic structures that give rise to back diffraction of light. In a 3D photonic crystal, illustrated in Fig. 22, light cannot propagate in any direction. As a result, photons can be trapped, as depicted in Fig. 23, where individual rods are selectively removed to form a high Q "cavity" within the 3D photonic crystal. Photonic crystals enable one to guide, store, switch and otherwise manipulate photons, in a manner similar to the way we now manipulate electrons, but with the added advantage that photon phase is detectable.

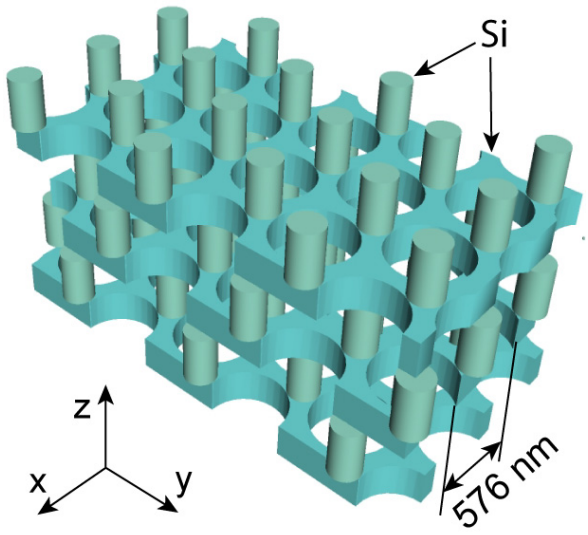

Figure 22: Schematic of the 3D photonic-crystal structure in Si, known as the "post and hole structure." In a 3D photonic crystal, back diffraction from the periodic structure prevents light from propagating in any direction, and over a rather large range of wavelengths. The corresponding range of optical frequencies for which propagation is not possible is called the "bandga." Such 3D structures lend themselves to fabrication via a membrane stacking.

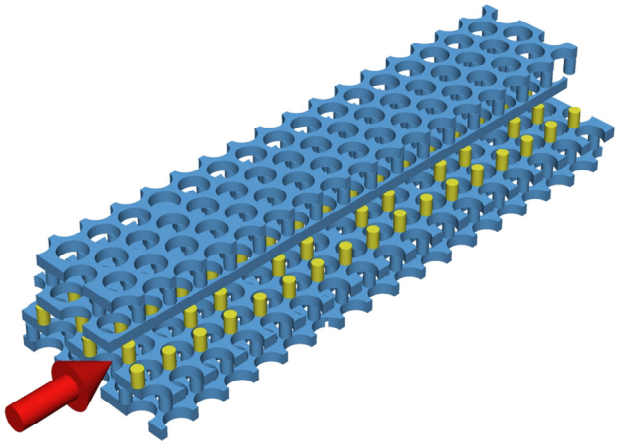

Figure 23: Sketch of a 3D photonic crystal in which selected posts have been removed, forming resonant cavities in which photons can be trapped. Adjacent cavities are weakly coupled, enabling photons to hop from one to the next, thereby propagating along the line of removed posts at a net speed that is slower than the normal speed of light. Such "slow-light" structures are of great interest for a number of applications from secure communication to phased-array radars.

The key issues with stacking of patterned membranes are: how to conduct nanopatterning on thin (of order 200 nm thick) membranes; how to clean such thin membranes; how to align the patterned membranes to form a stack; how to bond the stacked membranes; how to separate membranes from the frame that holds them without introducing fragments that would interfere with the bonding; and lastly, how to avoid membrane distortion.

We've developed a set of tools and techniques to address these problems. For nanopatterning, we conduct this operation while the membranes are mounted on a rigid substrate using lithographic techniques. For the specific application to 3-D photonic crystals, we developed a new tool called Coherent-Diffraction Lithography (CDL) illustrated in Fig. 24 and described in Ref. [1]. For cleaning membranes we found that megasonic cleaning is effective. Presumably the membranes survive because their resonant mechanical frequency is far removed from the megasonic frequency. For aligning membranes we employ interferometric-spatial-phase imaging (ISPI), developed originally for x-ray lithograph. For aligning the membranes of a 3D photonic crystals, we can also make use of the moire' patterns that form when one patterned membrane is placed on top of another.

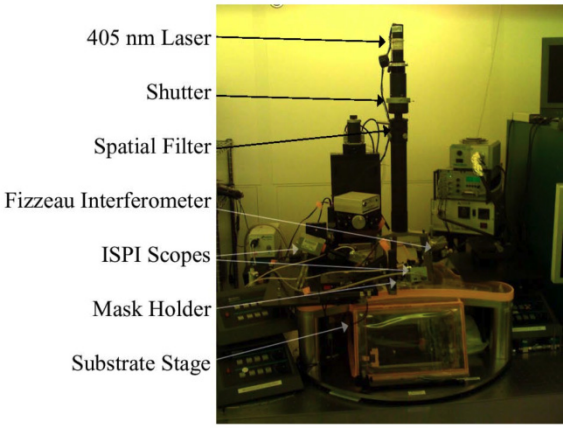

Figure 24: photograph of the Coherent-Diffraction-Lithography system developed for this project.

For bonding together the membranes that form a stack, we rely on van der Waals forces. However, at a later stage we may want to employ high temperature annealing, or to insert selected monolayers between membranes to aid bonding. To separate membranes from the frames that holds them without creating residues, we designed tethers that would cleave selectively, as depicted in Fig. 25. Membrane distortion is not a concern when the pattern is uniform and homogeneous, as it is for example in a single layer of a 3D photonic crystal. However, once we pattern deviations from perfect periodicity in a membrane layer of a 3D photonic crystal the tensile or compressive stresses within the membrane will cause differential strain, i.e., distortion. We are currently investigating an innovative approach that reduces the stress within the patterned membrane to essentially zero, which should result in zero or near-zero distortion.

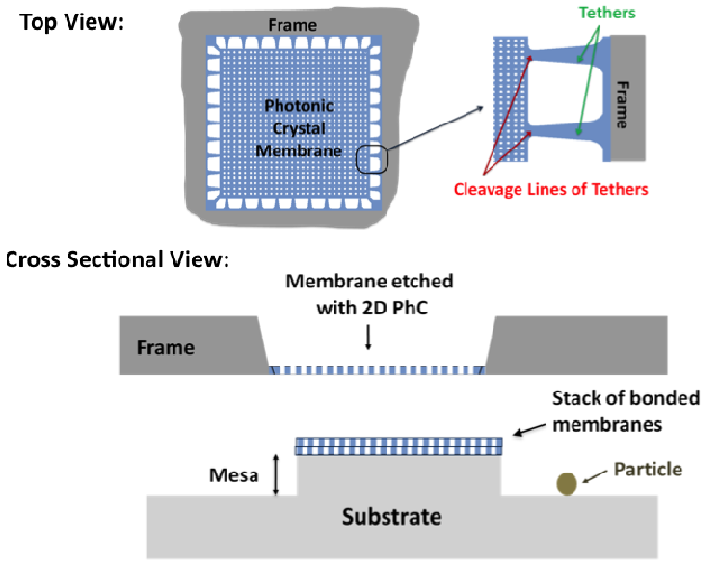

Figure 25: *(top) Schematic depicting a membrane with a photonic-crystal pattern, supported at the perimeter by tethers whose shape induces controlled cleavage. The cross-sectional view depicts the process of stacking the pre-patterned membranes to form a 3D photonic crystal free of particulate contamination.*

In order to produce the patterned membranes we first bond the semiconductor wafer, typically Si, to a glass substrate and then grind the Si down until only a micrometer or so thick. Then the Si is finely polished to achieve an optically smooth surface as well as the desired thickness. The Si is then patterned, and separated from its glass substrate by etching in a HF vapor, as depicted in Fig. 26. It is then ready for bonding as depicted in Fig. 25

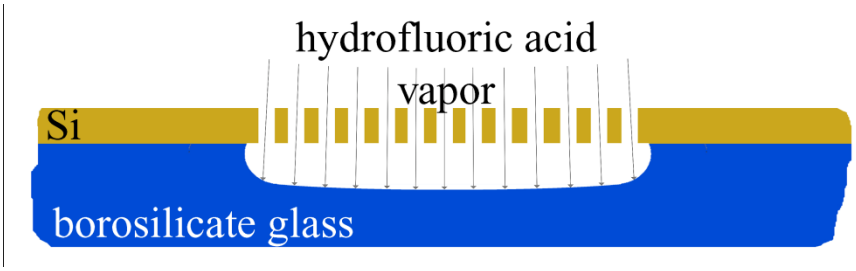

Figure 26: Depiction of formation of a patterned Si membrane held on a transparent glass frame.

References:
[1] A. Patel and H. I. Smith, "Membrane stacking: A New Approach for Three-Dimensional Nanostructure Fabrication," J. Vac. Sci. Techno. B 25, pp 2662-2664 Nov/Dec (2007).

[2] A. A. Patel, "Membrane Technology for the Fabrication of Three-Dimensional Photonic Crystals," Ph.D. Thesis, Dept. Electrical Engineering and Computer Science, Massachusetts Institute of Technology, Cambridge, MA. June, 2010.

Development of Superconducting Resonators for Quantum Coupling to Trapped Ions

Sponsor
DARPA

Project Staff
A. McCaughan, D. Meyer, S. Schulz, D. Aude, I. Chuang, K. K. Berggren
Department of Electrical Engineering and Computer Science, Massachusetts Institute of Technology

Over the last decade, quantum information experiments with trapped ions have demonstrated essential steps towards quantum computing and quantum simulation [1]. Large fields are required to achieve strong coupling to the ions via dipolar interactions. To accomplish this coupling, we are integrating transmission line microresonators into the 2D trap structures already implemented at the Center for Ultracold Atoms at MIT [2], [3]. The resonators are superconducting niobium to minimize-loss and maximize-quality factors [4]. Using the large fields locally generated from the accumulation of microwave photons in the resonator, we hope to demonstrate interaction with the trapped ions first by heating them, and eventually to control the rotational states of the ions by coherently coupling to them.

We fabricated the resonators as two-dimensional coplanar waveguides in niobium on R-plane sapphire using optical lithography. We deposited the niobium layers on the sapphire with an in-house DC magnetron sputtering system. The back side was thinly coated to create a ground plane, after which the front is coated to a thickness of approximately 400 nm. Tests showed that the niobium achieved superconductivity at the expected temperature of 9.2 K. Once we completed the material stack, we patterned the front niobium layer in NR9-3000P resist using optical lithography, developed it, and then reactive-ion etched it with CF4 and O2 to transfer the pattern into the niobium.

Current results from our fabricated resonators show first-resonance quality factors of at least 104 at 3.23 GHz and device temperatures of 3-4 K. In the near future we expect to see one or two orders of magnitude of improvement as we move from our probe-station testing apparatus to a full-immersion system to better isolate the devices and control temperature. In addition, we have prototyped designs to integrate resonators into existing superconducting traps.

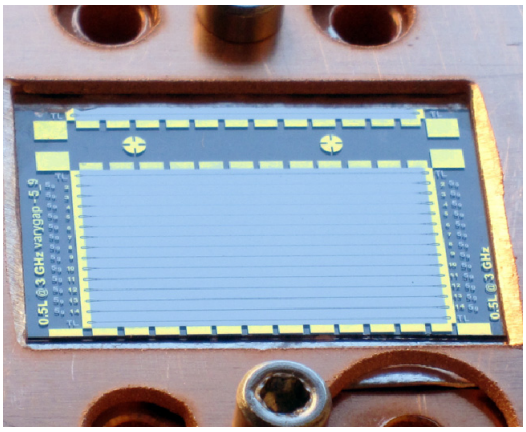

Figure 1: Resonators fabricated from niobium sputtered on sapphire. Each resonator is 20 mm in length and 11 um in width and has gold contact pads at either end for contact with the testing apparatus.

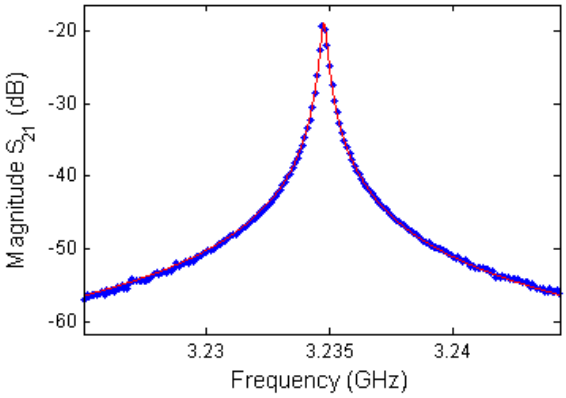

Figure 2: A Lorentzian fit to resonator transmission (S21) power measurements. The quality factor associated with the fit is 12,000.

References:

[1] A. André, D. DeMille, J. M. Doyle, et al. "A coherent all-electrical interface between polar molecules and mesoscopic superconducting resonators," Nature Physics, vol. 2(9), pp. 636-642, 2006.

[2] J. Labaziewcz, Y. Ge, P. Antohi, D. Leibrandt, K. Brown, and I. L. Chuang, "Suppression of Heating Rates in Cryogenic Surface-Electrode Ion traps," Phys. Rev. Lett. 100: 130001, 2008.

[3] D. Stick, W. Hensinger, S. Olmschenk, et al. "Ion trap in a semiconductor chip," Nature Physics, vol. 2(1), pp. 36-39, 2005.

[4] M. Göppl, A. Fragner, M. Baur, R. Bianchetti, S. Filipp, J. Fink, et al. "Coplanar waveguide resonators for circuit quantum electrodynamics," Journal of Applied Physics, vol. 104(11), pp. 3904, 2008.

Sub-5 keV Scanning-Electron-Beam Lithography

Sponsor

National Science Foundation and Center for Excitonics, an Energy Frontier Research Center funded by the U.S. Department of Energy, Office of Science (DE-SC0001088).

Project Staff

Lin Lee Cheong, Vitor R. Manfrinato, Huigao Duan, Donald Winston, Karl K. Berggren, Henry I. Smith.

Scanning-electron-beam lithography (SEBL) commonly uses voltages between 10-100 keV. Higher voltages result in distributed proximity effects, lower sensitivity, and a higher probability of substrate damage. Proximity effects raise concern because these effects limit resolution at voltages 10-50 keV, and complex and computationally-intensive programs are used to correct effects. Proximity effects can be reduced by using either very high voltages (100 keV) or very low voltages around 1 keV [1]. Our research efforts have investigated the feasibility of SEBL at energies of 2 keV and below.

Nested L's patterned in 15-nm-thick hydrogen silsesquioxane (HSQ) on silicon were used to investigate the resolution limit for dense patterns at low-voltages. L's at 20-nm pitch were sucessfully patterned at energies of 2 keV and 1.5 keV, as shown in Figure 1. At 1 keV energy, the finest pitch possible was 25 nm. Nested L's were also patterned in 11-nm-thick poly methyl methacrylate (PMMA) on silicon, with the minimum resolvable pitch at an energy of 2 keV being 70 nm. Monte-Carlo simulations of point-spread and line-spread functions were performed for a 2 keV, 9-nm diameter electron-beam incident on 15-nm-thick HSQ on silicon. The simulated distributed-energy-profile of dense L's is in agreement with experimental results. To demonstrate pattern-transfer capability of patterns fabricated with low-voltage SEBL, dense line patterns in HSQ were reactive-ion-etched (RIE) into XHRiC anti-reflective layer with HSQ as the etch mask. Figure 2 shows micrographs of ~9-nm-wide lines at pitches 30 nm and 40 nm successfully transferred to 60-nm-thick XHRiC.

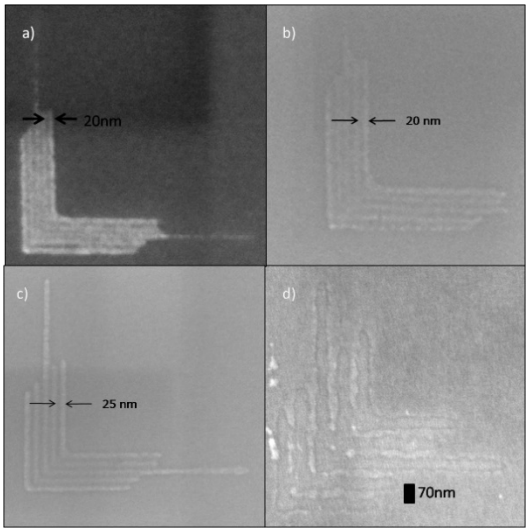

Figure 1: Scanning-electron micrographs of nested L's in 15-nm-thick HSQ patterned at electron energies of a) 2 keV, b) 1.5 keV, and c) 1 keV. The samples were developed in salty developer (4%NaCl, 1%NaOH in de-ionized water) for 60s. d) Scanning electron micrograph of nested L's in 11-nm-thick PMMA patterned at electron energy of 2 keV.

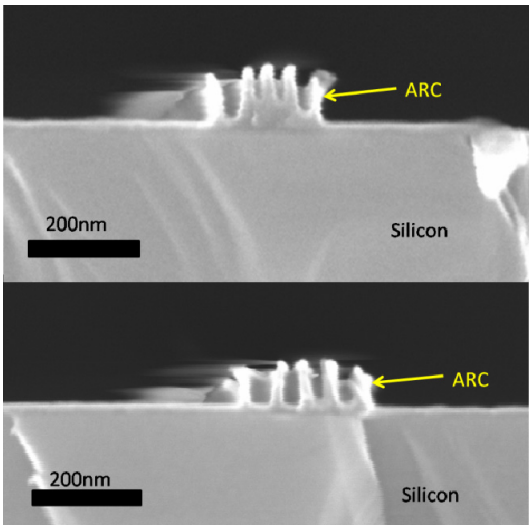

Figure 2: Scanning-electron micrographs of XHRiC cross-sections after reactive-ion-etching for 50s. Electron-beam lithography at an energy of 2 keV was used to pattern HSQ with lines. The HSQ lines was then used as a mask to transfer the pattern into XHRiC. Top micrograph shows the successful pattern transfer with lines at a 30-nm pitch, and the bottom micrograph is a cross-section of lines at 40-nm pitch. The lines are roughly 9-nm wide and the XHRiC approximately 60-nm thick.

Reference

[1] L.D. Jackel, R.E. Howard, P.M. Mankeiwich, H.G. Craighead, and R.W. Epworth, "Beam energy effects in electron beam lithography: The range and intensity of backscattered exposure," *Applied Physics Letters*, vol. 45, 1984, p. 698.

Publication

"Sub-5 keV Scanning-Electron-Beam Lithography," Vitor R. Manfrinato, Lin Lee Cheong, Huigao Duan, Donald Winston, Henry I. Smith, and Karl K. Berggren, submitted for publication, 2010.

Towards Observation of Single Nanocrystal Photoluminescence Emission in the Near-Infrared

Sponsors
Department of Energy, Air Force Office of Scientific Research

Project Staff
R. E. Correa, G. Nair, X. Hu, F. Marsili, E. Dauler, K. K. Berggren, M. G. Bawendi

The study of colloidal nanocrystals (NCs) that are optically active in the near-infrared is of great importance, from both a fundamental and technological perspective. Photoluminescence (PL) intermittency from single NCs has yet to be observed in materials that emit past 1 μm, largely due to the lack of single-photon-counting detectors in that wavelength regime. Similarly, an efficient room temperature single photon source at telecom wavelengths does not exist but remains highly desirable to many communities.

To meet these challenges, we have pursued studies on single core/shell indium arsenide (InAs)/cadmium selenide (CdSe) NCs whose photoluminescence can be tuned through the infrared [1]. Our motivation for choosing this system is two-fold: a) InAs PL lifetimes are relatively short, resulting in large single-photon bandwidths, and b) the shell improves the photostability of the single photon source by passivating defects on the surface of the core NC.

We have succeeded in imaging single or small-number clusters of InAs/CdSe NCs (Figure 1). NC emission was measured using a novel superconducting nanowire photo-detector capable of single-photon-counting with high efficiency [2], while scanning the sample position in the x-y plane to create a raster image. Preliminary PL intensity-versus-time traces of a single 'feature' do not display blinking, but this is most likely due to more than one NC being in the observation volume. An antibunching (g(2) intensity autocorrelation) experiment would confirm the presence of >1 NCs, and we are working towards this measurement on our apparatus.

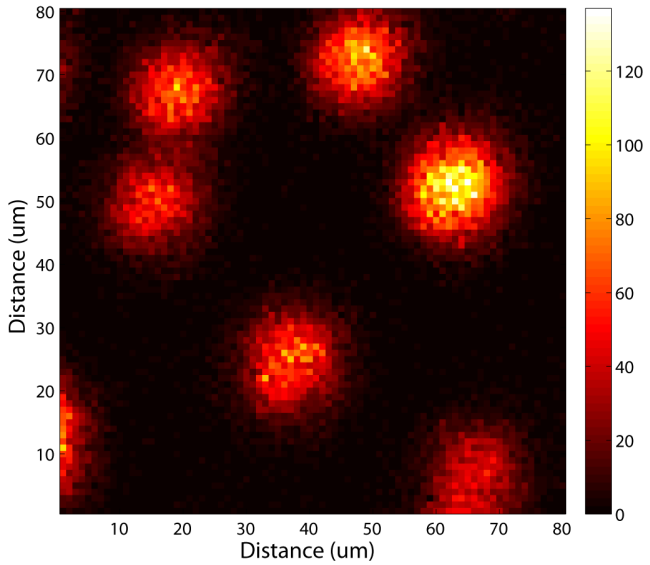

Figure 1: Confocal raster scan of a dilute InAs/CdSe nanocrystal film. The pixel size is 1 μm, and the emission was collected with 50 ms bin-times.

References

A. A. Guzelian, U. Banin, A. V. Kadavanich, X. Peng and A. P. Alivisatos, "Colloidal chemical synthesis and characterization of InAs nanocrystal quantum dots" *Applied Physics Letters,* vol. 69, pp. 1432-1434, September 1996

X. Hu, T. Zhong, J. E. White, E. A. Dauler, F. Najafi, C. H. Herder, F. N. C. Wong and K. K. Berggren, "Fiber-coupled nanowire photon counter at 1550 nm with 24% system detection efficiency" *Optics Letters,* vol. 34, pp. 3607-3609, December 2009

Optical Antenna-integrated Superconducting Nanowire Single-Photon Detectors

Sponsors
IARPA, NSF, AFOSR

Project Staff
X. Hu, E. A. Dauler, R. J. Molnar, K. K. Berggren

We designed and fabricated superconducting nanowire single-photon detectors (SNSPDs) with nano-optical antennae to reduce the length of the nanowire needed for efficient optical coupling. In our design, we increased the pitch of the meander and added a gold nano-optical antenna structure together with a top reflector to enhance the absorptance of the niobium nitride (NbN) nanowire for transverse-magnetically (TM) polarized incident light. This structure simultaneously suppressed the absorptance of transverse-electrically (TE) polarized light. The mechanism by which the antennae increase the absorption of TM-polarized light can be understood by modeling the structure as an array of slot waveguides. We experimentally demonstrated 47% device efficiency for a 9 μm × 9 μm, 600-nm pitch SNSPD for the TM-polarization and 4% for the TE-polarization, consistent with theoretical prediction. The reduction of the length of the nanowire shortened the detection efficiency recovery time for the detector after pulsing. The total length of the antenna-coupled nanowire was 145 μm. Compared with a typical (non-antenna coupled), 200-nm pitch SNSPD with the same area, the length of the nanowire was reduced by 2/3, and therefore the speed is expected to have been increased by a factor of 3.

At MIT Lincoln Laboratory, this work was sponsored by the United States Air Force under Air Force Contract #FA8721-05-C-0002. Opinions, interpretations, recommendations and conclusions are those of the authors and are not necessarily endorsed by the United States Government.

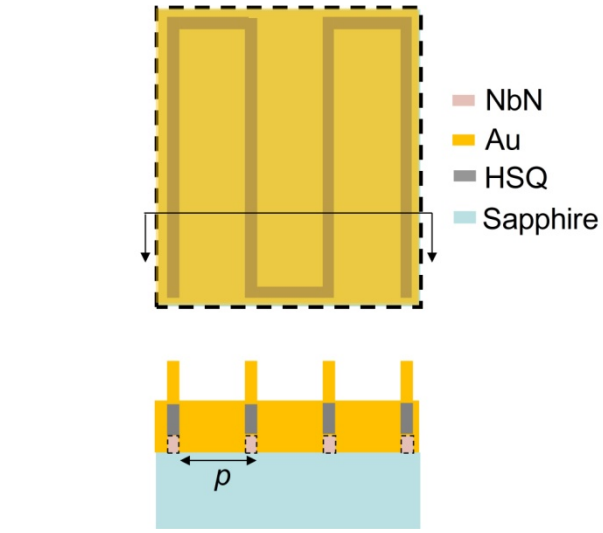

Figure 1: A schematic of optical-antenna-integrated superconducting nanowire single-photon detector. Compared with the design in the past[1], this design has gold structures between HSQ pillars to collect and focus light into NbN nanowire. The sparser meander with a pitch, *p*, makes the overall length of the nanowire shorter, yielding a faster detector.

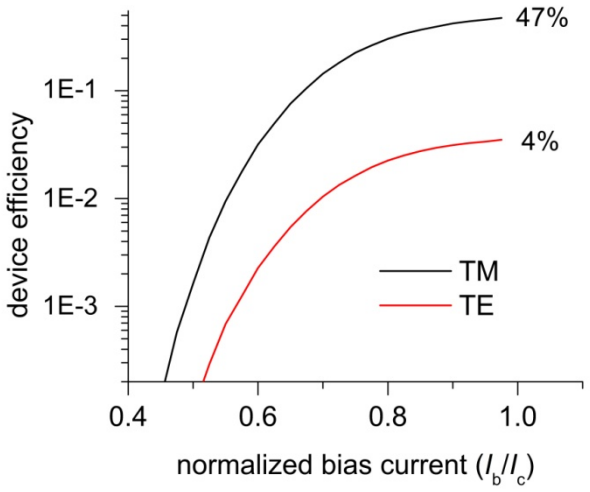

Figure 2: Measured device efficiency of the antenna-integrated superconducting nanowire single-photon detector for two polarizations.

Reference

K. M. Rosfjord, J. K.W. Yang, E.A. Dauler, A. J. Kerman, V. Anant, B. M. Voronov, G. N. Gol'tsman, and K. K. Berggren, "Nanowire single-photon detector with an integrated optical cavity and anti-reflection coating," *Optics Express*, vol. 14, issue 2, pp. 527-534, Jan. 2006.

Sub-10-nm Fabrication Based on Templated Self-assembly of Block Copolymer

Sponsor
ONR, NRI

Project Staff
Jae-Byum Chang, Jeong Gon Son, Prof. Caroline Ross, Karl K. Berggren

Templated block copolymer (BCP) self-assembly is attractive for fabricating few-nanometer-scale structures at high throughput [1]. Among several morphologies of block copolymer, cylindrical morphology has a big potential because it can be used for IC circuit fabrication. In our previous work, we fabricated complex structures that can be components of IC circuit by physically defined templates and self-assembled block copolymers [2]. We used polystyrene-polydimethylsiloxane (PS-PDMS) with a molecular weight (MW) of 45.5 kg/mol and a pitch of 36 nm. Because the pitch of cylindrical morphology block copolymer varies in direct proportion to its molecular weight, low-molecular-weight block copolymer is more desirable for making smaller structures.

Here, we applied the same strategy to low-molecular-weight block copolymer (MW 16 kg/mol) for making smaller structures. Figure 1a shows a scanning electron micrograph (SEM) of untemplated cylindrical morphology PS-PDMS whose molecular weight is 45.5 kg/mol. Compared with Figure 1a, Figure 1b shows much smaller structures made by lower-molecular-weight (MW 16 kg/mol) PS-PDMS. To template the self-assembly of low-molecular-weight PS-PDMS, the substrate surface was modified physically by hydrogen silsesquioxane (HSQ) and electron-beam lithography. After development, the surface of template was coated by PDMS monomer to attract PDMS blocks in PS-PDMS block copolymers. When the horizontal pitch is double the natural pitch of low- molecular-weight PS-PDMS, self-assembled cylindrical morphology PS-PDMS lines are aligned vertically (Figure 1c).

We also tried smaller templating posts whose diameter and height are less than 10 nm. A smaller post induces less strain to PS-PDMS block copolymer lines, so it is more desirable for templating low-molecular-weight block copolymer. To make such small posts, spin coated HSQ film was partially dissolved by MIBK, and then electron-beam lithography was carried out. SEM images of Figure 2 show vertically and horizontally aligned polymer lines depending on pitches.

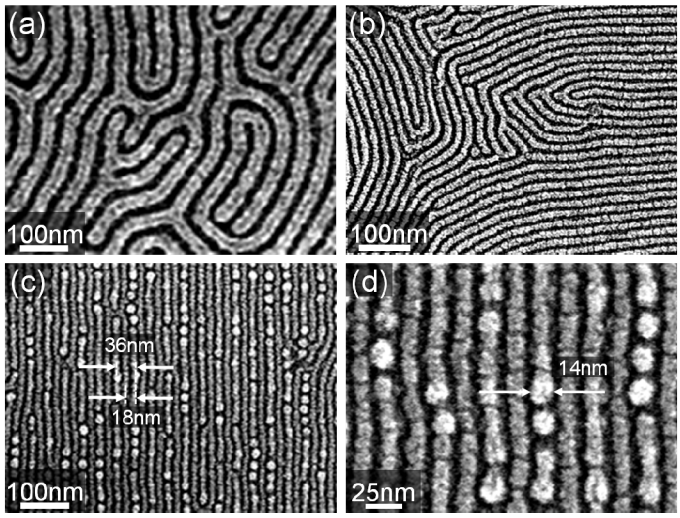

Figure 1: (a) SEM image of untemplated PS-PDMS (MW 45.5 kg/mol). (b) SEM image of untemplated PS-PDMS (MW16k). (c) Self-assembled low molecular weight PS-PDMS lines with templates. (d) Magnified image of Figure 1(c).

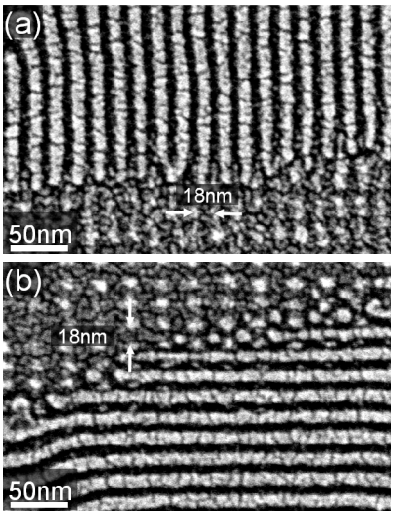

Figure 2: SEM image of self-assembled PS-PDMS (MW 16 kg/mol) lines templated by a smaller post when (a) the horizontal pitch is 18 nm (b) the vertical pitch is 18 nm.

References

[1] I. Bita, J.K. Yang, Y.S. Jung, et al., "Graphoepitaxy of self-assembled block copolymers on two-dimensional periodic patterned templates," *Science*, vol. 321, no. 5891, pp. 939-943, (2009).

[2] J.K. Yang, Y.S. Jung, J. Chang, et al., "Complex self-assembled patterns using sparse commensurate templates with locally varying motifs," *Nature Nanotechnology*, vol. 5, pp. 256-260, (2010).

Low-cost Lloyd's Mirror Interference Lithography

Sponsors

Singapore-MIT Alliance

Project Staff

H. Korre, C. P. Fucetola, J. A. Johnson, K. K. Berggren, Research Laboratory of Electronics, MIT

Periodic nanostructures have proven their usefulness in the fabrication of diffraction gratings, photonic crystals, magnetic domains in recording media, nanochannels in microfluidics [1], and even as templates for osteoblast migration [2]. Unfortunately the current tools to produce periodic nanostructures are enormous, are often difficult to operate, and cost anywhere from tens of thousands to millions of dollars. To address these issues, we devised a tool to produce periodic nanostructures with less complexity, less space, and less money.

Interference lithography is an ideal method for the rapid production of periodic nanostructures. The Lloyd's mirror interference lithography system uses a simple and rigid setup to produce one- and two-dimensional patterns, but its cost and size have previously been limited by the laser source (e.g., HeCd metal-vapor laser). Newly available low-cost blue laser diodes provide the ideal solution. They are small (about the size of a penny), can be controlled with a simple current source, and can cost as little as $300.

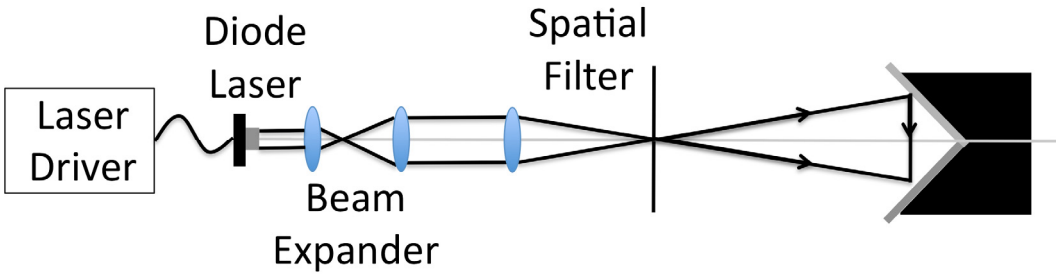

Figure 1: Tiny Lloyd's Mirror setup includes a laser driver, diode laser, beam expander, spatial filter, and mirror/substrate chuck. At the chuck, half of the beam is reflected from the mirror and subsequently interferes with a direct beam at the substrate. The interference of two beams creates a standing wave intensity pattern that is captured in a photosensitive material.

Using a commercially available blue laser diode, we have been able to solve the problems of size, complexity, and cost while maintaining the key functionality of the system. We previously presented our initial results [3] and have since improved the robustness of the tool. The Tiny Lloyd's Mirror is a tabletop system that can produce periodic nanostructures over a 1 cm^2 area. The tool also has the ability to control the spacing between nanostructures and produce one- and two-dimensional patterns. Figure 1 is a schematic of the Tiny Lloyd's Mirror tool. It consists of commercially available parts that are aligned in a linear fashion for easy construction. Figure 2 displays examples of the results that are achievable with the tool. Both one-dimensional gratings and two-dimensional rods are presented.

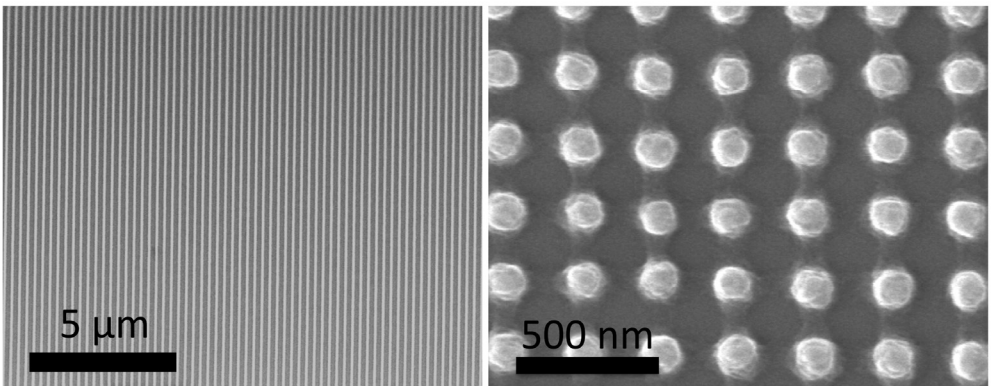

Figure 2: Scanning electron micrographs of one- and two-dimensional periodic nanostructures made with the Tiny Lloyd's Mirror. The gratings in the left image have a width of 131.5 nm while the rods in the right image have a diameter of 152.9 nm. The gratings have a pitch of 299.4 nm, which can be quickly modified by rotating the mirror/substrate chuck in Figure 1.

References

[1] S.R.J. Brueck, "Optical and Interferometric Lithography – Nanotechnology Enablers," *Proceedings of the IEEE*, vol. 93, no. 10, pp. 1704-1721, Oct 2005.

[2] E. Lamers et al., "The influence of nanoscale grooved substrates on osteoblast behavior and extracellular matrix deposition," *Biomaterials,* vol. 31, no. 12, pp. 3307-3316, Feb 2010.

[3] C.P. Fucetola, H. Korre, and K.K. Berggren, "Low-cost interference lithography," *Journal of Vacuum Science and Technology B*, vol. 27, no. 6, pp. 2958-2961, Nov/Dec 2009.

Sub-30-nm Patterning of Au on GaAs Substrates

Sponsor

NRI

Project Staff

J. Leu, M. Brewster, S. Gradecak, K. K. Berggren

In this work, we demonstrated the patterning of Au features on <111> B GaAs substrates by galvanic displacement and metal evaporation into sub-30-nm pores in a silicon oxide hard mask layer. Patterning of small Au features onto GaAs substrates is of particular interest due to their use as metal catalysts for GaAs and GaAs-alloy nanowire growth. Semiconducting nanowires have a variety of potential applications, such as field-effect transistors (FETs) [1], and their size-dependent properties have been exploited for a variety of optoelectronic devices [2]. However, much work remains to create lithographically-templated nanowires for integration into future manufacturing processes.

Gold in particular has shown promise in producing oriented, size-selected nanowires [3]. This research significantly improves on the smallest lithographically-fabricated catalyst-particle size, while suppressing unwanted nanowires by controlling the migration of metal particles during the growth process and by preventing the self-catalysis of GaAs nanowires from the GaAs substrate. Samples were prepared using GaAs substrates with 30 nm of evaporated silicon oxide deposited on top. The samples were patterned by electron-beam lithography, using a PMMA resist, and developed via a cold development process [4]. Pores were opened in the hard mask by HCF3/CF4 reactive-ion etching. After removal of the GaAs native oxide, metal catalyst

nanoparticles were deposited into the pores by either electron-beam evaporation of Au, with a nominal thickness of 3 nm, or by galvanic displacement (GD) in a calibrated solution that also deposits 3 nm of Au. The GD solutions were prepared by dissolving hydrogen tetrachloroaurate(III) trihydrate (Alfa Aesar Co.) into deionized (DI) water. With either method, the sub-30-nm gold nanoparticles were fabricated.

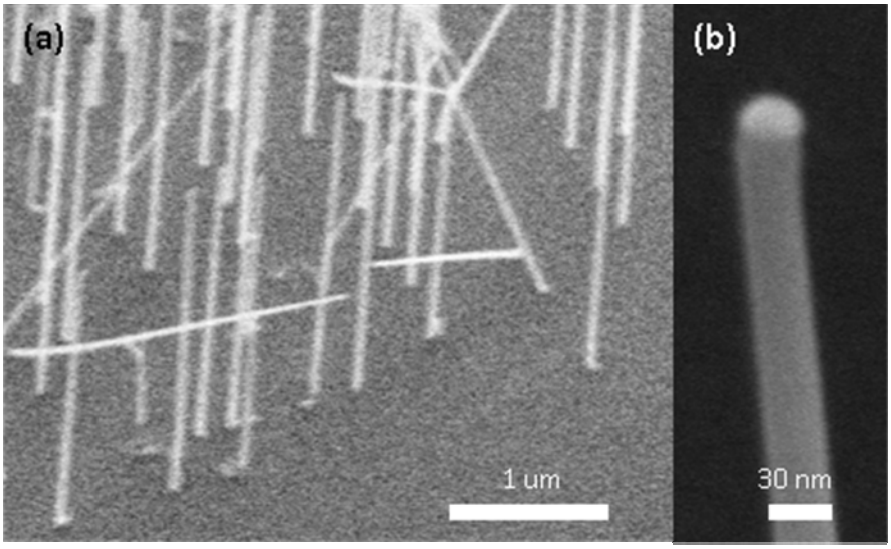

Figure 1: (a) An array of GaAs nanowires grown epitaxially by MOCVD, catalyzed by patterned Au/Cr metal features. (b) A 30-nm-diameter GaAs nanowire, with the metal catalyst clearly visible at the top of the nanowire.

References

[1] J. Goldberger, A.I. Hochbaum, R. Fan, and P. Yang, "Silicon vertically integrated nanowire field effect. Transistors," *Nano Lett., vol.* 6, p. 973, 2006.
[2] X. Duan, Y. Huang, Y. Cui, J. Wang, and C. M. Lieber, "Logic gates and computation from assembled nanowire building blocks," *Nature,* vol. 409, p. 66, 2001.
[3] P. Nguyen, H.T. Ng, and M. Meyyappan, "Growth of individual vertical germanium nanowires," *Adv. Mater.,* vol. 17, p. 1773, 2005.
[4] B. Cord, C. Dames, and K.K. Berggren, "Robust shadow-mask evaporation via lithographically controlled undercut" *J. Vac. Sci.Technol. B,* vol. 24, p. 3139, 2006.

Templated Self-assembly of Sub-10-nm Quantum Dots

Sponsors
MARCO MSD, NRI, IBM

Project Staff
J. Leu, B. Cord, P. Anikeeva, L. Battistella, J. Halpert, M. Bawendi, V. Bulovic, K. K. Berggren, Department of Electrical Engineering and Computer Science, Department of Materials Science and Engineering

Patterned templates can guide the self-assembly of nanoparticles into ordered arrays [1]. Our motivation in pursuing templated self-assembly is to develop a robust method for the creation of ordered structures at length scales below ten nanometers. The basic process entails creating surface-relief templates via electron-beam lithography and spin-coating a suspension of colloidal nanoparticles onto the template. These templates were created either via metal evaporation and

lift-off, or direct fabrication through the negative resist hydrogen silsesquioxane (HSQ). As the solvent evaporates, the quantum dots self-assemble primarily through the capillary forces created by the dewetting of the template [2].

We demonstrated this technique at sub-10–nm-length scales by spin-coating a solution of organically-capped CdZnS semiconducting quantum dots [3] onto nanopatterned grating structures on silicon substrates. We observed the geometric confinement of the quantum dots via physical templating and capillary forces into well-ordered monolayer aggregates with defined lattice orientations. While recent research has demonstrated the ability to self-assemble sub-10 nm metallic nanoparticles via capillary forces into physical templates of similar size [2], this work is unique in demonstrating lattice orientation control via physical templating at sub-10-nm-length scales.

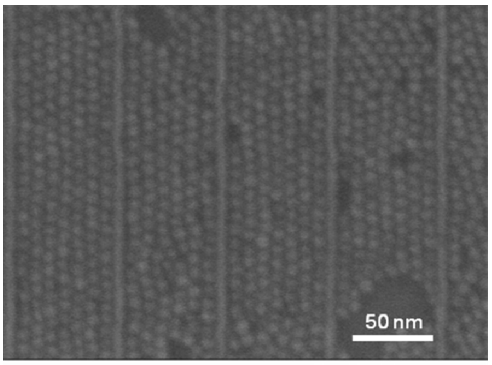

Figure 1: Scanning electron micrograph of a self-assembled quantum dot monolayer on a silicon substrate with lines formed by hydrogen silsesquioxane, on which 8-nm CdZnS quantum dots have self-assembled.

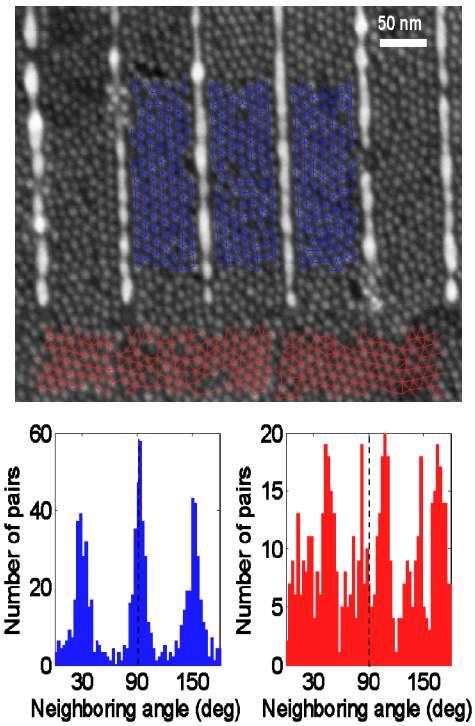

Figure 2: Image analysis of the template-imposed ordering. Superimposed on the image are the positional networks of selected areas. The templated areas (blue) clearly show positional ordering, while the untemplated regions (red) exhibit little ordering.

References

[1] Y. Yin, Y. Lu, B. Gates, and Y. Xia, “Template-Assisted Self-Assembly: A Practical Route to Complex Aggregates of Monodispersed Colloids with Well-Defined Sizes, Shapes, and Structures,” *J. Am. Chem. Soc.*, vol. 123, pp. 8718 8729, 2001.

[2] J.A. Liddle, Y. Cui, and P. Alivisatos, “Lithographically directed self-assembly of nanostructures,” *J. Vac. Sci. Technol. B.*, vol. 22, no. 6, pp. 3409-3414, Nov/Dec 2004.

[3] B. Fisher, J. M. Caruge, D. Zehnder, and M. Bawendi, "Room-Temperature Ordered Photon Emission from Multiexciton States in Single CdSe Core-Shell Nanocrystals," *Phys. Rev. Lett.*, vol. 94, p. 087403, 2005.

Superconducting Nanowire Single-photon-detectors Based on 30-nm-wide Nanowires

Sponsor
National Science Foundation, Department of Energy

Project Staff
F. Marsili, F. Najafi, X. Hu, C. Herder, E. Dauler, R. Molnar, K. K. Berggren
Department of Electrical Engineering and Computer Science, Lincoln Laboratory, Massachusetts Institute of Technology

In order to improve the sensitivity of superconducting nanowire single-photon-detectors (SNSPDs [1]) at telecom wavelengths and extend it to the middle infrared range, we fabricated SNSPDs based on 30-nm-wide nanowires (see Figure 1).

To make the photodetection pulse detectable with standard room-temperature electronics, *N* nanowires were arranged in a parallel architecture such that when one section fired, the current flowing through the whole device was redirected to the read-out circuitry (Superconducting Nanowire Avalanche Photodetector: SNAP) [2]. The signal-to-noise ratio was then *N* times higher than with a series design.

The single-photon detection efficiency (*DE*) of 30-nm-wide nanowire SNSPDs and of 2-, 3- and 4-section SNAPs was measured for 1550-nm wavelength at a temperature of 4.7 K. The *DE* exhibited a reduced dependence on the bias current (I_B) compared with 100-nm-wide SNSPDs. This reduced dependence allowed operating narrow SNSPDs at an I_B (~ 50 % of the critical current I_C) far lower than with wide SNSPDs (typically ~ 95 % of I_C) for the same *DE*. This reduction in the operating bias current would in principle improve the detector sensitivity, as the dark count rate (*DK*) of SNSPDs decreases exponentially with I_B. However, the highest *DE* measured at 0.5 I_C was 7% for a *DK* = 100 Hz, which does not represent an improvement to the sensitivity of wide SNSPDs. This performance occurred in part due to the low fill factor (f = 30 %) of the device's active area, due to the high operating temperature, and due to the background-radiation-induced dark counts.

The work at Lincoln Lab was sponsored by the United States Air Force under Air Force Contract #FA8721-05-C-0002. Opinions, interpretations, recommendations and conclusions are those of the authors and are not necessarily endorsed by the United States Government.

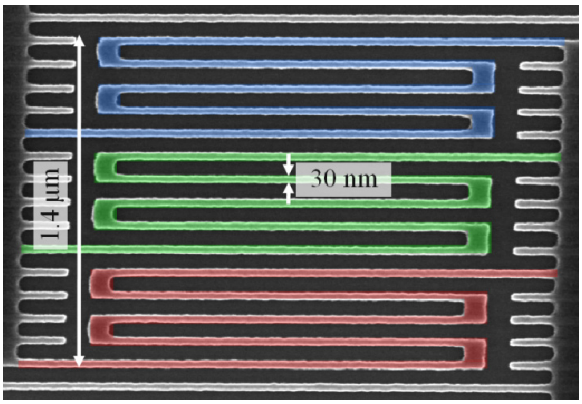

Figure 1: Scanning electron microscope (SEM) images of the hydrogen silsesquioxane (HSQ) mask of a 3-section SNAP. The nanowires are 30 nm wide and are arranged in a meander pattern with 100-nm pitch. This structure was obtained by electron-beam lithography (30 kV acceleration voltage) on 45-nm-thick HSQ.

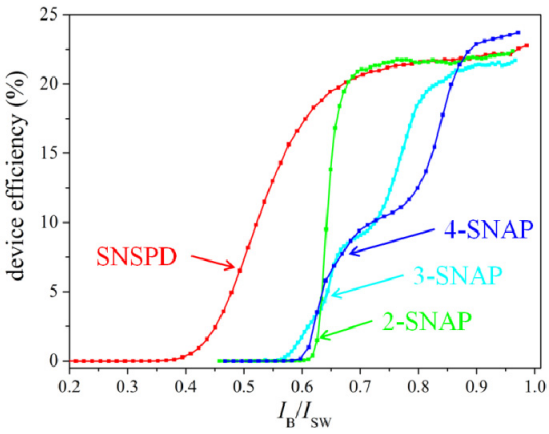

Figure 2: Plot of the detection efficiency as a function of the normalized bias current for an SNSPD and for a 2-, 3- and 4-SNAP. The nanowires are 30 nm wide.

References

[1] G.N. Gol'tsman *et al.*, "Picosecond superconducting single-photon optical detector," *Appl. Phys. Lett.,* vol. 79, pp. 705, 2001.

[2] M. Ejrnaes *et al.*, "A cascade switching superconducting single photon detector,"*, Appl. Phys. Lett.,* vol. 91, pp. 262509, 2007.

Point Spread Function for PMMA as a Negative Resist

Sponsors
The University of the South, NSF

Project Staff
R. S. Peterson, H. Duan, K. K. Berggren
The University of the South
Research Laboratory of Electronics, MIT

Poly(methyl methacrylate) (PMMA) is an important resist for electron-beam lithography. For low doses, it is a positive resist; for high doses, a negative resist. Knowledge of the point-spread function (PSF) is critical for proximity effect corrections (PEC) using electron-beam lithography with PMMA as a negative-tone resist [1]. An example of the positive- and negative-tone PMMA is shown in Figure 1.

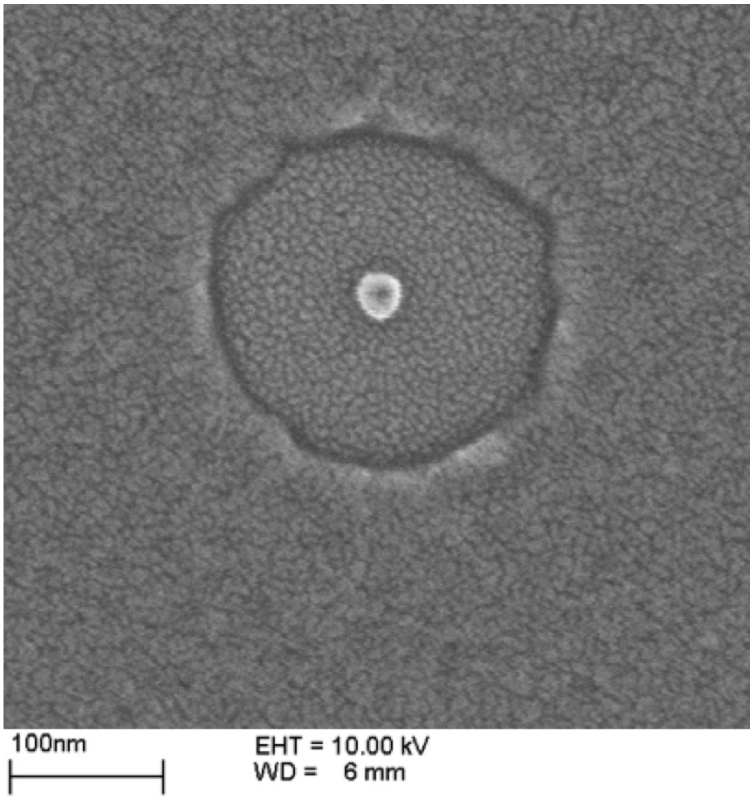

Figure 1: SEM image of a beam spot at 10 keV and a dose of 760 fC. The hole's diameter from the positive-tone response of the PMMA is 215 nm, and the diameter of the center pillar, produced by the negative tone PMMA is 27nm.

Sequences of single-point exposures are made in 40-nm PMMA at doses high enough to produce the negative resist behavior for electron energies of 2-30 keV. Development at 30°C in a mixture (2:1) of isopropyl alcohol and methyl isobutyl ketone yields center posts increasing in diameter with increasing dose. The PSF is determined from these measurements. The results for 10-keV electrons are shown in Figure 2. The PSF function is usually modeled as the sum of two or more Gaussian functions. One Gaussian represents the effects of forward-scattered electrons and another represents the back-scattered electrons. Four Gaussians are used to model the data in Figure 2. The fit for the forward scattering is not well determined from the data because a 4.5-nm radius is the smallest feature size reliably measured.

A Monte Carlo simulation, including the effects of secondary electrons, is in good agreement with the measured PSF of Figure 2. It is used to improve the fit for forward scattering. The good agreement between the Monte Carlo simulation and the positive and negative resist PSFs in Figure 2 suggests that there is no significant difference in the physical interactions of the electrons with the PMMA resist to produce a positive- or a negative-tone effect other than total dose. The differences visible in the measured PSFs may be primarily due to a change in the density of the resist with dose, an effect not included in the Monte Carlo model.

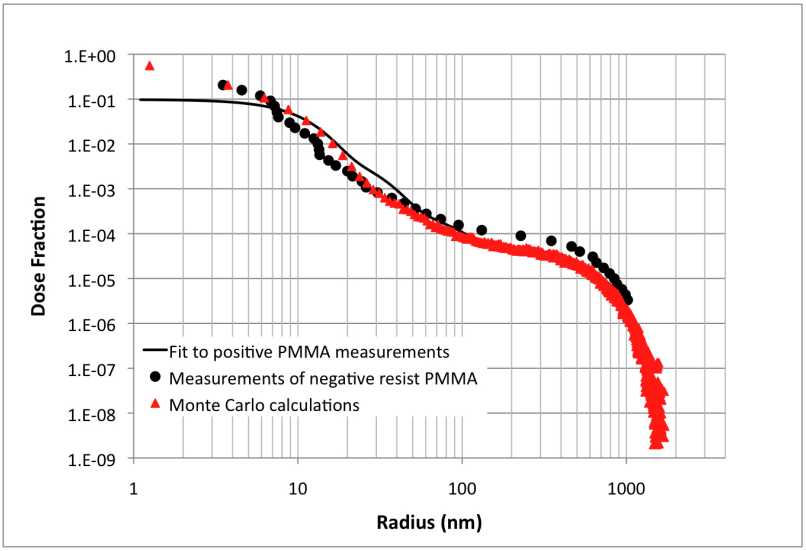

Figure 2: Measurements and Monte Carlo calculations of the point spread functions for 10 keV electrons on 40 nm-thick PMMA. The PSFs for the positive- and negative-tone PMMA are scaled to overlay the normalized Monte Carlo PSF values. The fit to the positive-resist data is used for clarity.

References

[1] H. Duan, J. Zhao, Y. Zhang, E. Xie, and L. Han, "Preparing patterned carbonaceous nanostructures directly by overexposure of PMMA using electron-beam lithography," *Nanotechnology*, vol. 20, 135306, 2009.

Electrochemical Development of Sub-10-nm-pitch Hydrogen Silsesquioxane (HSQ) Structures in Saline Solution

Sponsor
Alfaisal University and King Abdulaziz City for Science & Technology, ONR

Project Staff
S. Strobel, K. Harry, H. Duan, K. K. Berggren
Research Laboratory of Electronics, MIT

A new method for developing hydrogen silsesquioxane (HSQ), a negative electron-beam resist with demonstrated 9-nm-pitch resolution [1], is presented, avoiding the addition of hydroxyl ions to the developer. This method addresses and possibly overcomes physical and chemical factors influencing the achievable resolution of HSQ during development [2].

The development mechanism of the acidic-like resist HSQ in basic solution is assumed to be the conversion of HSQ into negatively charged, water-soluble ions under the generation of hydrogen, simplified as: $\equiv Si{-}H + OH^- \rightarrow \equiv Si{-}O^- + H_2$. Thereby the Si-H bound of the HSQ is transformed into a $Si\text{-}O^-$ configuration that is chemically more favorable for the basic pH value of the developer solution. But the transition of Si–H to Si–OH and even into $Si{-}O^-$ also occurs in water under normal circumstances, although with slim probability. We enhance this reaction by applying a potential between sample and solution, thereby enforcing an electrical current.

We have demonstrated the development of HSQ in non-alkaline saline solution (4% NaCl in DI-water) and applied potential of about 2.5V and achieved comparable resolution to salty development (1% NaOH and 4% NaCl in DI-water) with pattern dimensions as good as 9-nm-pitch nested-L structures, see Figure 1 and 2. Development was observed only at the negative electrode and with applied potential. Therefore we hypothesize that the unexposed resist is either directly reduced to negatively charged HSQ ions by the transfer of electrons or water is electrolyzed and thereby developer is locally produced on the resist.

Electrochemical development of resist opens a new pathway for development that is not limited by diffusion and possible charging of the sample surface. Furthermore, the negatively charged resist ions are repelled by the substrate. The speed and quantity of development can be adjusted by the applied potential.

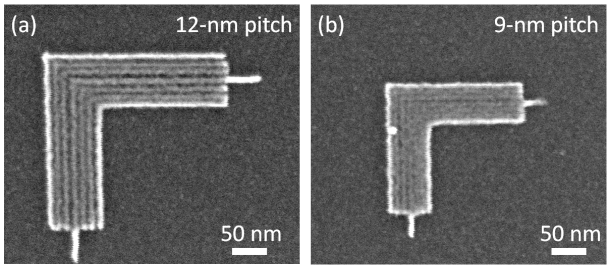

Figure 1: SEM images comparing electrochemical development with salty development of 9-nm-pitch (a) and 12-nm-pitch (b) nested-L structures patterned in ~15-nm-thick HSQ on silicon. Experiments demonstrated comparable resolution of electrochemical development and salty development of HSQ and no obvious influence of the substrate (silicon and silicon coated with a thin chrome layer) on the development quality.

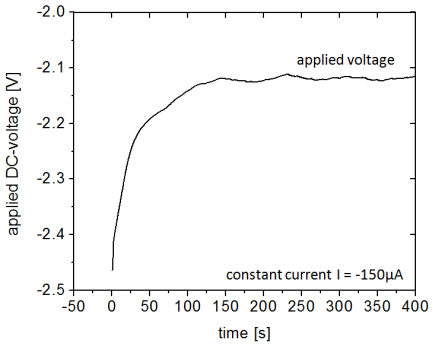

Figure 2: Time evolution of applied potential between a sample with chrome coating and saline solution during electrochemical development for a constant current of I = -150µA. At the beginning, the HSQ resist acted as high-resistive layer on the sample surface, and thus a larger potential had to be applied. With proceeding development, the applied potential decreased as more and more chrome surface was exposed until the resist was removed from the complete surface and a steady current value was reached.

References

[1] J.K.W. Yang, B. Cord, K.K. Berggren, J. Klingfus, SW. Nam, KB. Kim, and M.J. Rooks, "Understanding of hydrogen silsesquioxane electron resist for sub-5-nm-half-pitch lithography," *Journal of Vacuum Science & Technology B,* vol. 27, no. 6, pp. 2622-2627, 2009.

[2] B. Cord, J. Yang, H.G. Duan, D.C. Joy, J. Klingfus, and K.K. Berggren, "Limiting factors in sub-10 nm scanning-electron-beam lithography," *Journal of Vacuum Science & Technology B,* vol. 27, no. 6, pp. 2616-2621, 2009.

Simulated secondary-electron trajectories in helium-ion-beam lithography

Sponsors
NRI, NSF GRFP

Project Staff
D. Winston, J. Ferrera, K. K. Berggren; Research Laboratory of Electronics, MIT

Scanning helium-ion-beam lithography (HIBL) can fabricate patterns with sub-10-nm half-pitch [1, 2]. The interaction volume of a beam with a sample is one measure of the spatial extent of energy deposition in that sample, and thus of lithographic resolution. To evaluate limits on the interaction volume of a helium-ion beam and its generated secondary electrons (SEs) inside a resist layer, we have developed a Monte Carlo simulator using the software of Ziegler et al [3], a parametric model for SE generation by helium ions [4], and models for propagation of primary and "fast secondary" electrons [5, 6].

Figure 1 suggests that the contrast-reducing proximity effect, common in dense patterns written with ≥10-keV electron-beam lithography (EBL), is absent for 30-keV HIBL. The interaction volume of the helium-ion beam is smaller than that of the electron beam, and no helium ions backscatter to the hydrogen silsesquioxane (HSQ) resist layer. HSQ was chosen for this simulation because of its status as a high-resolution EBL resist [7], because experiments by the authors – using HSQ – correspond with our electron model [8], and because HSQ has been used for sub-10-nm-half-pitch HIBL [1, 2].

Figure 2 suggests that, at least for resist thicknesses larger than a few nm, 30-keV HIBL can pattern smaller features than ≤30-keV EBL. This is because the helium-ion beam does not fan out with depth as rapidly as the electron beams do (Figure 2(a)). However, it seems that SE generation limits the interaction diameter of the helium-ion beam to ~ 2 nm because the helium-ion beam generates more SEs closer to the surface than do the electron beams (Figure 2(b)).

Our simulations suggest that HIBL may ultimately prove superior to EBL in the effort to simultaneously minimize (1) the proximity effect and (2) feature size, both of which limit resolvable half-pitch in resist-based lithography.

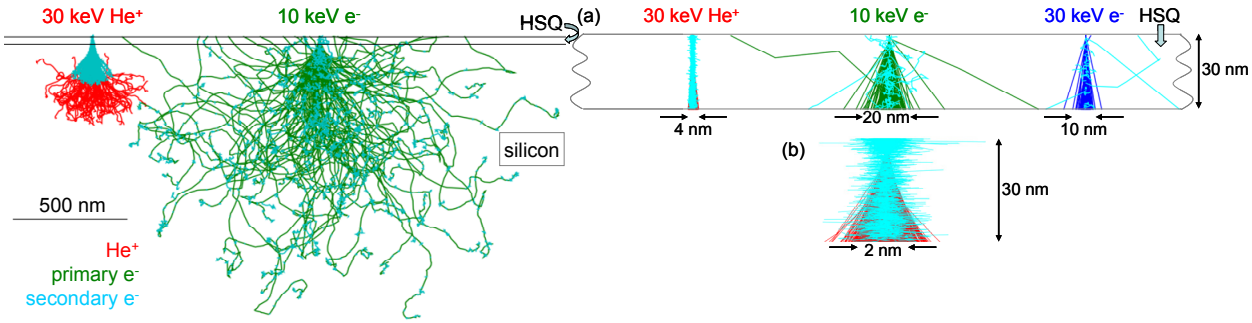

Figure 1: Simulated trajectories of 100 30-keV helium ions (left) and 100 10-keV electrons (right), into 30-nm-thick hydrogen silsesquioxane (HSQ) resist on silicon. 10-keV electron landing energy was chosen because this is a typical low-end value for electron-beam lithography. The trajectories of secondary electrons generated by each particle beam are also simulated and plotted (light blue).

Figure 2: (a) Simulated trajectories (1000 each) of 30-keV helium ions (left), 10-keV electrons (center), and 30-keV electrons (right), and also those of the secondary electrons generated by each beam (light blue), in a 30-nm-thick "membrane" of hydrogen silsesquioxane (HSQ) resist. No trajectories are tracked below the HSQ, and thus no backscattered particles emerge from below the HSQ. Vertical and lateral scales are equal; (b) Magnified graphic of the 30-keV helium ions (red) and their generated secondary electrons (light blue), where the lateral scale is stretched relative to the vertical scale to emphasize the SE tracks.

References

[1] D. Winston, B. M. Cord, B. Ming, D. C. Bell, W. F. DiNatale, L. A. Stern, A. E. Vladar, M. T. Postek, M. K. Mondol, J. K. W. Yang and K. K. Berggren, "Scanning-helium-ion-beam lithography with hydrogen silsesquioxane resist," *J. Vac. Sci. Technol. B,* vol. 27, pp. 2702-2706, 2009.

[2] V. Sidorkin, E. van Veldhoven, E. van der Drift, P. Alkemade, H. Salemink and D. Maas, "Sub-10-nm nanolithography with a scanning helium beam," *J. Vac. Sci. Technol. B,* vol. 27, pp. L18-L20, 2009.

[3] J. F. Ziegler, J. P. Biersack and M. D. Ziegler, *SRIM–The Stopping and Range of Ions in Matter.* Chester, MD: SRIM Co., 2008.

[4] R. Ramachandra, B. Griffin and D. Joy, "A model of secondary electron imaging in the helium ion scanning microscope," *Ultramicroscopy,* vol. 109, pp. 748-757, 2009.

[5] R. A. Ghanbari, "Physics and fabrication of quasi-one-dimensional conductors," Doctoral thesis, Massachusetts Institute of Technology, Cambridge, 1993.

[6] D. C. Joy, *Monte Carlo Modeling for Electron Microscopy and Microanalysis.* New York: Oxford University Press, 1995.

[7] J. K. W. Yang, B. Cord, H. Duan, K. K. Berggren, J. Klingfus, S. Nam, K. Kim and M. J. Rooks, "Understanding of hydrogen silsesquioxane electron resist for sub-5-nm-half-pitch lithography," *J. Vac. Sci. Technol. B,* vol. 27, pp. 2622-2627, 2009.

[8] L. Batistella, D. Winston, J. Ferrera, M. Mondol and K. K. Berggren, in preparation.